An integrin centered complex coordinates ion transport and pH to regulate f-actin organization and cell migration in breast cancer.

Chiara Capitani[1*], Jessica Iorio[1*], Elena Lastraioli[1], Claudia Duranti[1], Giacomo Bagni[1], Ginevra Chioccioli Altadonna[1], Rossella Colasurdo[1,2], Giorgia Scarpellino[3,4], Scott P. Fraser[5], Andrea Becchetti[6], Mustafa B. A. Djamgoz[5,7] and Annarosa Arcangeli[1#]

[1]Department of Experimental and Clinical Medicine, University of Florence, Florence, Italy

[2] Department of Medical Biotechnologies, University of Siena, Italy

[3] Department of Life Sciences and Systems Biology, University of Turin, Turin, Italy

[4] Department of Biology and Biotechnology "L. Spallanzani", University of Pavia, Pavia, Italy

[5] Imperial College London, Department of Life Sciences, London, United Kingdom

[6] Department of Biotechnology and Biosciences, University of Milano Bicocca, Milan, Italy

[7] Biotechnology Research Centre, Cyprus International University, Haspolat, TRNC, Mersin 10, Türkiye

[*]Equally contributed

[#]Correspondence: annarosa.arcangeli@unifi.it, Phone: +39 055 2751-319/283/285; Fax: +39 055 2751281

Running title: NHE1/hERG1/β1 integrin/nNa$_V$1.5 in breast cancer

Keywords: ion channels, transporters, cell adhesion, Fibronectin, filopodia, invadopodia intracellular pH, triple negative breast cancer

ABSTRACT

The cross talk between the Microenvironment (TME) and cancer cells controls proliferation, migration and pro-metastatic cancer behavior, often through integrin-mediated cell adhesion to the Extracellular Matrix (ECM). Integrin receptors coordinate signaling hubs constituted by multiprotein plasma membrane complexes often comprising ion channels and transporters. We here describe a novel signaling pathway triggered by β1 integrin activation by the ECM protein fibronectin (FN). This pathway involves a β1 integrin-centered plasma membrane complex formed by different transport proteins: the hERG1 K^+ channel, the neonatal form of the Na^+ channel Na_V 1.5 (nNa_V1.5) and the Na^+/H^+ antiporter NHE1. The NHE1/hERG1/β1/nNa_V1.5 complex is present on the plasma membrane of Breast Cancer (BCa) cells, in particular Triple Negative Breast Cancer (TNBCa). The expression of the two ion channels present in the complex is mutually regulated. The complex engagement by cell adhesion to FN stimulates a NHE1-mediated cytoplasmic alkalinization, which modulates f-actin organization. This in turn controls TNBCa migration and invasiveness. All this pathway is impaired by blocking either hERG1 or nNa_V1.5 which also cause complex disassembly. The same result is obtained by harnessing the hERG1/β1 integrin complex through a single chain bispecific antibody (scDb-hERG1-β1).

In conclusion, we uncovered a plasma membrane complex that recruits different ion transport proteins that regulate cellular K^+, Na^+ and H^+ fluxes and cooperate in modulating downstream signals and thus malignant behavior. This complex could be targeted to develop novel therapeutic strategies for one of the most difficult-to-treat cancers, i.e. TNBCa.

INTRODUCTION

Dysregulation of cell migration promotes the development of invasion and metastasis in cancer (Yamaguchi and Condeelis, 2007) and represents one of the hallmarks of cancer (Hanahan and Weinberg, 2011). Cell motility is initiated in response to growth factors or chemokines that stimulate the formation of plasma membrane protrusions whose direction is regulated by local Ca^{2+} levels (Small et al, 2002; Pollard and Borisy, 2003). These protrusions, in the form of lamellipodia or filopodia, are driven by the polymerization of f-actin which not only represents a simple regulator of mechanical properties of the cell but also behaves as a platform for signaling pathways (Moujaber and Stochaj, 2020). In metastatic cancer cells membrane protrusions are organized in special structures named invadopodia which allow to cross physiological barriers and in turn to trigger the metastatic process (Yamaguchi and Condeelis, 2007). All the above structures that are linked to cell motility and invasion are stabilized by adhesions to Extracellular Matrix (ECM) proteins through specific cell receptors. In these processes, integrins are pivotal since they link the plasma membrane to the f-actin cytoskeleton (Vogel et al, 2006; Dufort et al, 2011) but also transduce intracellular signaling pathways hence working as bidirectional signal transducers (Hynes et al, 2002).

Integrin receptors coordinate intracellular signaling through the formation of plasma membrane hubs constituted by multiprotein plasma membrane complexes which often comprise ion channels and transporters (Becchetti et al, 2019). Wide evidence is now available for the *human ether-á-go-go-related gene* (hERG1) K^+ channel, encoded by the *KCNH2* gene. The complex between the β1 integrin subunit and hERG1 is highly present in cancer cells and operates as a supramolecular signaling hub (Duranti & Iorio et al, 2023). The complex modulates cell migration through the re-organization of f-actin in PDAC and CRC cells (Duranti & Iorio et al, 2023). In CRC cells ECM-triggered, integrin-mediated cell migration also depend on intracellular alkalinization through an increased H^+ efflux via the Na^+/H^+ exchanger NHE1 (Iorio et al, 2020).

hERG1 is also expressed in Breast Cancer (BCa) cells (Fukushiro-Lopes et al, 2017; Breuer et al, 2019) and primary samples (Iorio et al, 2018). In the Triple Negative Breast Cancer (TNBCa) cell

line MDA-MB-231 hERG1 is physically associated with the β1 integrin subunit, to form a hERG1/β1 integrin complex which enhances the metastatic potential *in vivo* (Becchetti et al, 2017). BCa cells and primary samples also show an upregulation of the 1.5 subtype of Voltage Dependent Sodium channels ($Na_V1.5$) encoded by the *SCN5A* gene. In BCa cells, and in particular in TNBCa cells, $Na_V1.5$ promotes invasiveness and metastasis (Roger et al, 2003; Fraser et al, 2005) through mechanisms which also involve the Na^+/H^+ exchanger NHE1 (reviewed in Luo et al, 2020). Interestingly, BCa cells preferentially express the neonatal splice variant of $Na_V1.5$, which potentiates BCa cell invasiveness *in vitro* (Brackenbury et al, 2007).

The present paper was aimed at studying the hERG1/β1 integrin complex in BCa cells and how it regulates the f-actin cytoskeleton and cell migration. We found that the complex (i) is present in several BCa cell lines, (ii) its formation is triggered by cell adhesion to the ECM protein FN and (iii) recruits both the neonatal form of the Na^+ channel Na_V 1.5 ($nNa_V1.5$) and the Na^+/H^+ antiporter NHE1. The NHE1/hERG1/β1/$nNa_V1.5$ complex is present on the plasma membrane of BCa cells, in particular in TNBCa. The expression of the two ion channels present in the complex is mutually regulated. The complex engagement by cell adhesion to FN stimulates a NHE1-mediated cytoplasmic alkalinization, which modulates f-actin organization. This in turn controls TNBCa migration and invasiveness. All this pathway is impaired by blocking either hERG1 or $nNa_V1.5$ which also cause complex disassembly. The same result is obtained by harnessing the hERG1/β1 integrin complex through a single chain bispecific antibody (scDb-hERG1-β1).

RESULTS

A hERG1/β1 integrin macromolecular complex is present in BCa cells of different molecular subtype

We previously showed that a hERG1/β1 integrin complex is present on the plasma membrane of cancer cells, including MDA-MB-231 BCa cells (Becchetti et al, 2017). We first studied whether this complex was present in different BCa cells, analyzing four human cell lines with different molecular characteristics: MCF-7 (luminal A, weakly metastatic), SKBR3 (HER2 positive, weakly metastatic), MDA-MB-468 and MDA-MB-231 (TNBCa, strongly metastatic) (Kao et al, 2009). All the analyses were done on cells seeded for 2 hours on fibronectin (FN) as in Duranti & Iorio et al, 2023. We first determined the levels of the *KCNH2* transcript (by RQ-PCR) and of the hERG1 protein by WB and IF. For IF we used a specific antibody recognizing an extracellular epitope of the channel (mAb-hERG1, Table S1). *KCNH2* was expressed in all the cells at varying levels: MDA-MB-468 and MDA-MB-231 cells showed the highest levels, while SKBR3 and MCF-7 cells the lowest (**Figure 1A**). The hERG1 protein was expressed in all the native BCa cell lines at comparable level (**Figure 1B**). When the plasma membrane localization of the channel was analyzed by IF, MDA-MB-468 cells showed the highest levels, MCF-7 the lowest and MDA-MB-231 and SKBR3 intermediate levels (**Figure 1C**). Proteins from all the cell lines were immunoprecipitated with either a monoclonal antibody recognizing extracellular epitopes of the β1 integrin (mAb-TS2/16) (IP: β1 integrin) or the mAb-hERG1 (IP:hERG1). Polyclonal antibodies directed against intracellular epitopes of the two proteins were used to label the WBs (**Figure 1D**). Co-immunoprecipitation (co-IP) data were quantified by densitometry as detailed in Materials and Methods (see the bar graph showing the densitometric data on the right of Figure 1D). Overall, a hERG1/β1 integrin complex occurs in BCa cells once seeded on FN for 2 hours, especially in TNBCa cells. As previously shown in PDAC and CRC cells (Duranti & Iorio et al, 2023), also in BCa cells the complex was sensitive to (meaning was dissociated by) treatment with either the classical hERG1 blocker E4031 or the bispecific antibody which specifically targets the hERG1-β1 integrin complex (scDb-hERG1-β1). This was evident from either co-IP

(**Figure 1E**) or IF experiments, where the fluorescence intensity obtained after labeling the complex with scDb-hERG1-β1 was determined (**Figure 1F**). Both treatments reduced the complex formation, although the effect of scDb-hERG1-β1 was stronger. Data relative to TNBCa cells MDA-MB-231 and MDA-MB-468 are in **Figure 1C**, data relative to MCF-7 and SKBR3 cells are shown in Supplementary Figure 1A).

We then determined the localization of the hERG1/β1 integrin complex in BCa cells. We first focused on focal adhesions (FAs), i.e. pivotal localization of integrins (Wozniak et al, 2004), testing whether the hERG1/β1 integrin complex co-immunoprecipitated/co-localized with paxillin (Ibata et al, 2020). Indeed, co-IPs revealed the presence of paxillin in the β1 integrin IPs containing hERG1 (**Figure 2A**). Co-localization of hERG1 and paxillin, evidenced by IF experiments, was quantified as the Manders' Overlapping Coefficient (MOC). Indeed hERG1 (**Figure 2B**, upper panels, and related MOC values on the bottom of each picture) as well as the complex, labelled with a bispecific antibody recognizing the hERG1/β1 integrin complex, scDb-hERG1-β1, Table S1 (Duranti & Iorio et al, 2023) (**Figure 2B**, lower panels, and related MOC values on the bottom of each picture.) with paxillin. We then studied whether the hERG1/β1 integrin complex in FAs recruited cytoskeletal proteins such as vinculin, α-actinin 1 or f-actin (Otey et al, 1993, Takahashi, 2001). Neither f-actin nor vinculin were present in the co-IP of hERG1 and β1 integrin, while α-actinin1 co-immunoprecipitated with the β1 integrin and hERG1 in all the four cell lines, in particular in TNBCa cells (**Figure 2A**). Silencing hERG1 and immunoprecipitating the proteins with mAb-TS2/16 did not affect the co-IP with α-actinin (**Figure 2C**), whereas silencing β1 and immunoprecipitating with the mAb-hERG1 resulted in the withdrawal of both α-actinin1 and hERG1 from the complex (**Figure 2D**).

In conclusion, the hERG1/β1 integrin complex is present in BCa cells, especially in TNBCa, localizes in FAs with paxillin and recruits α-actinin1, which is linked to the β1 integrin (**Figure 2E**).

The hERG1/β1 integrin macromolecular complex recruits nNa$_V$ channels in BCa cells: the hERG1/β1/nNav1.5 complex

Given the high expression and relevant role of Na$_V$ channels in BCa cells (Fraser et al, 2005; Brisson et al, 2013), we analyzed weather the hERG1/β1 integrin complex recruited the Na$_V$1.5 channel protein in BCa cells. We followed the same procedure as above, first determining the levels of the *SCN5A* transcript (by RQ-PCR) and of the Na$_V$1.5 protein by WB and IF. In particular we quantified the expression of either the adult or the neonatal form of the channel, *aSCN5A* and *nSCN5A*, the latter been expressed in BCa cells (Brackenbury et al, 2007). While *aSCN5A* was hardly detectable, the expression of *nSCN5A* was higher amongst the native cells. MDA-MB-468 and SKBR3 showed a higher expression level compared to MDA-MB-231 and MCF-7 cells (**Figure 3A**). The expression of the two transcripts in HEK cells stably transfected with either the two *SCNA5* cDNAs (EBNA-aNa$_V$1.5 and EBNA-nNa$_V$1.5 cells, respectively) are also shown in **Figure 3A**. Since *nSCN5A* was dominant we investigated only this isoform in the following experiments. The expression levels of nNa$_V$1.5 protein were determined by WB and IF, using a newly developed antibody specific for nNa$_V$1.5 (Duranti et al, personal communication, February 2024) which recognizes an extracellular epitope of the channel (mAb-nNa$_V$1.5, Table S1). The WB data showed the presence of two bands: a band weighing 227 kDa and a band of higher molecular weight (~245 kDa). According to what described for the adult form of Na$_V$1.5 (Baroni et al, 2017) the two bands correspond to the partially or un-glycosylated, immature form and to the fully glycosylated, mature form of the protein, respectively. All BCa cell lines expressed the protein in comparable levels when quantified (**Figure 3B**). The presence and plasma membrane localization of the channel was confirmed by IF. With this technique MDA-MB-231 and MDA-MB-468 cells showed the highest levels, MCF-7 the lowest (**Figure 3C** and the bar graph on the right).

We therefore asked whether nNav1.5 could also be an additional component of the hERG1/β1 integrin macromolecular complex. Thus, co-IP (**Figure 3D**) and co-localization (**Figure 4A**) experiments were performed on all the BCa cells. For co-IP we used either the mAb-TS2/16 (IP: β1 integrin) or

the mAb-hERG1 (IP:hERG1). The mAb-nNa$_V$1.5 was then used in the WBs to detect the nNa$_V$1.5 protein and the co-IPs were quantified by densitometry as detailed in Materials and Methods (**Figure 3D**). Both hERG1 and nNa$_V$1.5 co-immunoprecipitated with β1 integrin, in different proportions in the cell lines (see the bar graph showing the densitometric data below **Figure 3D**). The two TNBCa cells, showed the highest expression levels of the three proteins. IF experiments, employing the two monoclonal antibodies (one directed against hERG1 and the other against nNa$_V$1.5) and quantifying the co-localization as MOC, confirmed that hERG1 and nNa$_V$1.5 co-localized in BCa cells seeded for 2 hours on FN (**Figure 4A**). Silencing either hERG1 or the β1 integrin led to an important difference in the expression of other proteins. In fact, silencing hERG1 produced a decrease in the expression of nNa$_V$1.5 (**Figure 4B**), while silencing β1 integrin resulted in the complete withdraw of both hERG1 and nNa$_V$1.5 (**Figure 4C**). MDA-MB-468 cells showed the highest overlap (MOC = 0.76 ± 0.04) meaning the highest co-localization of the two channels. Finally, IF experiments also showed that nNa$_V$1.5 co-localized with paxillin, meaning the presence of the channel in FA, as the hERG1/β1 integrin complex (**Figure 4D**).

In conclusion, a tri-molecular complex hERG1/β1/nNa$_V$1.5 occurs in FAs of BCa cells, especially TNBCa cells, once seeded on FN for 2 hours (**Figure 4E**).

hERG1 and nNa$_V$1.5 are mutually "controlled" in BCa cells

Since hERG1 and Na$_V$1.5 form a microtranslatome in the heart (Eichel et al, 2019), we tested whether the two channels were linked at the translational level also in BCa cells. To this purpose, we analyzed the effects of either silencing the two channels separately or overexpressing one of the two channels, in particular overexpressing hERG1 (Becchetti et al, 2017). As already observed from data shown in Figure 3F, silencing hERG1 induced a decrease in nNa$_V$1.5 expression by 40-45%, in MCF-7 and SKBR3, and by 55% ca in TNBCa cell lines, in addition to the disappearance of the hERG1 protein (**Figure 5A**). Silencing nNa$_V$1.5 resulted in the disappearance of the nNa$_V$1.5 protein, accompanied

by a decrease of hERG1 expression by 45% in both MCF-7 and SKBR3, and by 55% ca. in the TNBCa cell lines (**Figure 5B**).

The over-expression of *KCNH2* in MDA-MB-231 cells (giving MDA-MB-231-T cells) produced a significant over-expression of both *KCNH2* and *nSCN5A* transcripts (**Figure 5C**). These results were also observed at the protein level (WB data are in **Figure 5D**, IF data are in Supplementary Figure S5A) as well as in the recorded specific currents (**Figure 5E**). Indeed I_{hERG1} was 98.8 ± 26.4 pA with a current Density (pA/pF): 4.5 ± 1.4 (N = 5 cells) and $I_{nNaV1.5}$ was172.8 ± 20.2 pA with a current density (pA/pF): 8.7 ± 2.3 (N = 5) cells in MDA-MB-231 WT; in MDA-MB-231-T I_{hERG1} was 2673.0 ± 143.0 pA with a current density (pA/pF): 116.2 ± 32 (N = 5 cells) and $I_{nNaV1.5}$ was 478.2 ± 69.8 pA with a current density (pA/pF): 18.45 ± 2.8 (N = 8 cells). Overall, the hERG1 and $nNa_V1.5$ channels are mutually controlled in BCa cells, at both the transcription and translation level, similarly to what occurs in the heart (Eichel et al, 2019). This result was further stressed analyzing the effects of the two specific blockers of hERG1 (i.e. E4031) and of $Na_V1.5$ (i.e. TTX). The treatment with E4031 decreased the expression of both hERG1 and $nNa_V1.5$ by 45% ca. in MCF-7 and SKBR3 and by 55%-60% in TNBCa cell lines (**Figure 6A**). The treatment with TTX decreased the expression of both $nNa_V1.5$ and hERG1 by 40% in both MCF-7 and SKBR3 and by 55%-60% in the TNBCa cell lines (**Figure 6B**). Overall, the two channel blockers decreased the expression of the two channel proteins with a stronger effect in the TNBCa cell lines (see the bar graphs with the densitometric data on **Figure 6C**). Finally, both E4031 and TTX decreased the level of the hERG1/β1/$nNa_V1.5$ complex to the same extent, although a clear trend it's shown where E4031 decreases the complex more than TTX. In addition to that the effect is clearly higher in the two TNBCa cell lines (**Figure 6D** and the bar graphs with the densitometric data in **Figure 6E**).

The hERG1/β1/nNav1.5 complex controls f-actin organization

Based on the role of the hERG1/β1 integrin complex in PDAC and CRC cells (Duranti & Iorio et al, 2023), we then studied the involvement of the hERG1/β1 integrin complex in f-actin organization of

BCa cells. To this purpose, Bca cells were seeded on FN for two hours, fixed and processed for IF to determine (i) the expression and recruitment of the Arp2/3 complex (i.e. the first step of f-actin enucleation (Swaney & Li, 2016; Johnston et al, 2008); (ii) the organization of f-actin in stress fibers and filopodia, using rhodamine conjugated phalloidin as in Duranti & Iorio et al, 2023; (iii) the emission and quantification of invadopodia, staining the cells with an anti-cortactin antibody (Weaver et al, 2001). To determine the role of the complex, we treated BCa cells with E4031, TTX or the scDb-hERG1-β1, since all these treatments reduced complex formation (see Figure 1E, 1F and 5D), although the effect of scDb-hERG1-β1 was stronger.

The fluorescence intensity of Arp2/3 significantly increased at the plasma membrane level (see the white masks in Figure 2C) when MDA-MB-231 and MDA-MB-468 were treated with E4031, and even more with TTX or scDb-hERG1-β1 compared to controls (**Figure 7A**). This indicates that the Arp2/3 complex moves from the cytoplasm to peripheric areas, possibly those where amoeboid protrusions (filopodia) are formed (see below). No difference in the localization of Arp2/3 was seen in MCF-7 and SKBR3 when treated with either E4031, TTX or scDb-hERG1-β1 (Supplementary Figure S7A). Both E4031 and TTX reduced the length of stress fibers by roughly 50% and 55%, respectively. The treatment with scDb-hERG1-β1 had an even stronger effect (**Figure 7B** and the bar graph on the bottom). The length and density of filopodia were also increased by all the treatments (**Figure 7B** and the bar graph on the bottom). TTX and scDb-hERG1-β1 had the strongest effect (30-40%). A similar increase was observed by all the treatments on the density of cortical actin (**Figure 7B** and the bar graph on the bottom). Also in this case TTX and scDb-hERG1-β1 had the strongest effect (40-45%). The staining with the anti-cortactin antibody showed a clear, punctate pattern in the two TNBCa cell lines (**Figure 7C**). In contrast, cortactin staining was weak and diffuse and only few, faint spots were detected in both MCF-7 and SKBR3 cells (Supplementary Figure S7B). The Invadopodia Index (InvI) value was reduced by E4031 (roughly 55%) and even more by TTX (65%) and scDb-hERG1-β1 (roughly 60%) in MDA-MB-231 and MDA-MB-468 cells (**Figure 7C** and the

bar graph on the right). No significant effect was seen in MCF-7 and SKBR3 (Supplementary Figure S7C).

Overall, these data indicate that the hERG1/β1/nNa$_V$ 1.5 integrin complex regulates the organization of f-actin in TNBCa cells, keeping the stress fibers spread and neatly grouped, and the filopodia retracted, to allow the organization of f-actin in invadopodia.

The signaling pathways downstream to the hERG1/β1/nNa$_V$1.5 complex:

We then studied the intracellular signaling pathways which is triggered by the hERG1/β1/nNav1.5 complex and regulates f-actin organization in the different structures of the cytoskeleton. We first focused on (i) intracellular Ca^{2+} (Manoli et al, 2019) and (ii) AKT (Becchetti et al, 2017; Duranti & Iorio et al, 2023). These experiments were performed on MDA-MB-468 (which had the highest levels of the complex and on MCF-7 cells which showed the lowest (see Figure 1D and 3D). The basal value of the intracellular calcium concentration ($[Ca^{2+}]_i$) was significant higher in MDA-MB-468 cells compared to MCF-7 (Figure 7A), but no effect of plating on FN or treating the cells with either channel blocker in either cell line was observed (**Figure 8A**). No effects in either cell lines treating with either channel blockers or the scDb-hERG1-β1 was also observed in the levels of AKT phosphorylation (pAKT), as determined by both WB (**Figure 8B**) and IF (Supplementary Figure S8B).

Given the relevant role of pH (both extracellular, pHe, and intracellular, pHi) on f-actin organization and hence cancer cell migration and progression (Moolenaar WH, 1986, Denker SP & Barber DL, 2002, Frantz C et al, 2008) and the role of pHi in the hERG1-dependent regulation of cell migration in colorectal cancer cells (Iorio et al, 2020), we studied pHi in our model. Compared with the initial value (T0) , pH_i increased significantly in all the cells when plated on FN for 2h (**Figure 8 C**, pink vs white bars): 7.013 ± 0.002 to 7.135 ± 0.001 (in MCF-7 cells), 7.042 ± 0.001 to 7.171 ± 0.002 (in SKBR3 cells), 7.052 ± 0.003 to 7.253 ± 0.002 (in MDA-MB-231 cells) and 7.081 ± 0.001 to 7.283 ± 0.003 (in MDA-MB-468 cells). Thus, the FN-induced intracellular alkalinization was higher (by

ca. 15%) in the TNBC cells. No change was seen in cells seeded on BSA control (**Figure 8C**, black bars). E4031 and TTX equally reduced the FN-induced alkalinization of pH_i, especially in the TNBC cells, while scDb-hERG1-β1 had a significantly stronger effect. We then tested whether the Na^+/H^+ antiporter NHE1 was involved in the above pHi alkalinization. Indeed, the specific NHE1 inhibitor cariporide completely blocked the effect of cell adhesion to FN on pHi, decreasing pH_i to levels lower than those measured at T0 or in cells seeded on BSA (**Figure 8C**). Overall, NHE1 is the main responsible of pHi regulation in BCa cells, and in particular in the FN-induced alkalinization observed in TNBCa.

We then investigated whether NHE1 was present in the hERG1/β1/$nNa_V1.5$ macromolecular complex. Indeed, the antiporter co-immunoprecipitated with β1 integrin, hERG1 and $nNa_V1.5$ (**Figure 9A and B**). Interestingly the antiporter was absent when hERG1 was transiently silenced, indicating its binding to the K^+ channel protein (**Figure 9A)**. On the other hand, silencing β1 did not result in the absence of NHE1 showing that its binding is not related to the β1 integrin (**Figure 9B**). Hence, the complex can be addressed as "NHE1/hERG1/β1/nNaV1.5 complex. The presence of NHE1 antiporter in the complex turned out to be relevant in the FN-induced f-actin organization, since the treatment with cariporide decreased stress fiber length and increased filopodia length (**Figure 9C**), similarly to what was observed with the E4031, scDb-hERG1-β1 and TTX treatments. Again, these effects were stronger in TNBCa cells MDA-MB-231 and MDA-MB-468 (**Figure 9D**; Supplementary Figure S8C).

Overall, these data show that a NHE1/hERG1/β1/$nNa_V1.5$ regulates pHi and affects f-actin organization in TNBCa cells (**Figure 9D**).

The hERG1/β1 integrin/$nNa_V1.5$ complex promotes TNBCa cell migration and invasiveness.

We then analyzed the contribution of the NHE1/hERG1/β1/nNav1.5/NHE1 complex to cell proliferation, lateral motility and Matrigel invasion of the four cell lines We tested the effects of (i) E4031, (ii) TTX and (iii) scDb-hERG1-β1 which similarly impaired the formation of the complex.

Neither treatment had any effect on proliferation (**Figure 10A**). In contrast, both E4031 and TTX significantly inhibited the lateral motility of MDA-MB-468 and MDA-MB-231 cells, reducing MoI by ca. 50% after 24h (**Figure 10B**). The effect of scDb-hERG1-β1 was even stronger compared to the two blockers reducing MoI by roughly 55%. Cariporide reduced cell motility (a reduction of MoI of 75% was observed), and the strongest effect (reduction of MoI of 85%) was obtained by the combination of Cariporide and scDb-hERG1-β1. The motilities of the MCF-7 and SKBR3 cells were only slightly or not affected by E4031, TTX, scDb-hERG1-β1, cariporide or the combination of cariporide and scDb-hERG1-β1 (**Figure 10B**). Similar observations were made in experiments lasting 48h (Supplementary Figure S9A).

As regards Matrigel invasion, E4031, TTX, scDb-hERG1-β1 and cariporide were significantly inhibitory on MDA-MB-231 and MDA-MB-468 cells (ca. 40% and 40%; 40% and 45%; 45% and 45%; 50% and 50%; 60% and 60% respectively) after 16h (**Figure 10 C**). Also in this case, the combination of cariporide and scDb-hERG1-β1 showed the strongest inhibitory effect on Matrigel invasion. Only a slight or no effect were observed on SKBR3 and MCF-7 cells with all the above treatments.

DISCUSSION

Cancer metastases often represent the main obstacle to successfully treat solid cancer, especially those hard-to-treat-cancers such as Triple Negative Breast Cancer (TNBCa). The pro-metastatic behavior which characterizes malignant cells is regulated by the cross talk between the Tumor Microenvironment (TME) and cancer cells. This often occurs through integrin-mediated cell adhesion to ECM proteins, which triggers pro-migratory, and hence pro-metastatic signaling pathways. In this context, integrin receptors coordinate signaling hubs constituted by multiprotein plasma membrane complexes often comprising ion channels and transporters. In the present paper, we uncovered a novel signaling pathway triggered by β1 integrin activation by the ECM protein FN in BCa cells, in particular in TNBCa. This pathway involves a β1 integrin-centered plasma membrane macromolecular complex comprising a potassium (hERG1) and a sodium (nNa_V1.5) ion channel, the Na^+/H^+ transporter NHE1 and the cytoskeletal actin-binding protein α-actinin1. The expression of the two ion channels present in the complex is mutually regulated. The complex engagement by cell adhesion to FN stimulates a NHE1-mediated cytoplasmic alkalinization, which modulates f-actin organization. This in turn controls TNBCa migration and invasiveness. This apparently occurs both directly, through α-actinin1 and indirectly, through the NHE1-mediated alkalinization of intracellular pH. In any case, the role of the two channels is pivotal, being the signaling pathway and its functional consequences fully regulated by the two channels. This is witnessed by the inhibitory effects of two channel blockers, i.e. E4031 and TTX, as well as by RNA silencing. The same result is obtained by harnessing the hERG1/β1 integrin complex through a single chain bispecific antibody (scDb-hERG1-β1) (**Figure 11**).

The signaling pathway triggered by the hERG1/β1/nNa_V1.5 macromolecular complex: the striking role of pHi in the regulation of f-actin organization

The macromolecular complex we discovered in BCa cells is centered on the β1 subunit of integrin receptors, is triggered by cell adhesion to the ECM protein FN, is localized in nascent focal adhesions

and exploits the β1 integrin as central hub. All these features stress the role of the TME in regulating BCa cell behavior, in particular the migration process which underlies cancer metastasis (Koedoot et al, 2019). Besides the integrin, the macromolecular complex comprises two different ion channels (the hERG1 potassium and the $nNa_V1.5$ sodium channels) as well as an ion transporter (the Na^+/H^+ exchanger NHE1) and α-actinin. The two latter proteins are relevant in triggering downstream functional effects, in particular cell migration (Iorio et al, 2022). The non-muscle α-actinin isoforms behave as actin-binding proteins and are necessary for the proper organization and customized functioning of the cytoskeleton. In addition, α-actinins are associated with focal contacts and stress fibers and can serve as scaffold proteins to connect the plasma membrane to the actin cytoskeleton and to diverse signaling pathways (Sjoblom et al, 2008). In BCa cells α-actinin1 is bound to β1 integrins (Takahashi, 2001) and its expression is elevated in TNBCa cell lines where it is involved in the rearrangement of the actin cytoskeleton and related cell migration (Kovac et al, 2018). Furthermore, α-actinin is a direct target of the integrin-dependent Focal Adhesion Kinase (FAK) in platelets (Izaguirre et al, 2001) and is highly sensitive to pH values higher than 7 (Condeelis and Vahey , 1982). When phosphorylated by FAK or in the presence of an alkaline pH, α-actinin loses its actin binding property (Noegel et al,1987) which has a clear impact in enhancing cell motility (Sjoblom et al, 2008). All these conditions realize in our cellular model. In addition, NHE1 activity affects both pHi and pHe leading to alkalinization of pHi and acidification of pHe, which characterize cancer cells (White et al,2017). Both effects control cancer cell behaviors, in particular cancer cell migration (Liu et al, 2020). In particular, it was proposed that $Na_V1.5$ promotes MDA-MB-231 BCa cell migration and invasion through a NHE1-dependent peri-membrane acidification, which consequently promotes the activity of acidic cathepsins (Gillet et al, 2009, Brisson et al, 2011). Interestingly, $Na_V1.5$ and NHE1 co-localize in caveolin-1-rich plasma membrane domains (Brisson et al, 2013), further stressing the functional relevance of macromolecular plasma membrane complexes in the control of cellular pH. In our model, however, the effects of pH are mainly related

to the organization of f-actin cytoskeleton. It is known that f-actin remodeling can transform into different subcellular structures (filopodia, lamellipodia, and stress fibers), regulated by different signaling pathways (Gardel et al, 2010). In our system, the NHE1/hERG1/β1/nNa$_V$1.5 complex apparently converge to keep TNBC cells in a configuration more prone to starting the migration process.

The occurrence and functional relevance of ion channels working within plasma membrane macromolecular complexes both in normal and in pathological contexts, is emerging so far (Heijman et al, 2018; Ponce-Balbuena et al, 2018; Eichel et al, 2019). An intriguing difference between ion channel complexes in normal vs pathologic, e.g. cancer, cells is the presence in the latter of interacting proteins which are relevant for cancer signaling (Becchetti et al, 2022, Arcangeli et al, 2023). Besides the hERG1/β1 integrin complex that is selectively expressed in cancer cells (Becchetti et al, 2017; Arcangeli A et al, 2024), also Orai1/TRPC1/SK3 Potier-Cartereau et al, 2022), K$_V$10.1/Calmodulin (Marques-Carvalho et al, 2016) Kv10.1/Orai1/SPCA2 (Badaoui et al, 2018; Peretti et al, 2019) as well as SWELL (LRRC8A)/integrin (Kang et al, 2018) complexes have been discovered. These macromolecular complexes are widely involved in different aspects of cancer cell behaviour that depend on cell adhesion to ECM proteins (Qiu et al, 2014; Gunasekar et al, 2019; Alghanem et al, 2021). The occurrence of a NHE1/hERG1/β1/nNa$_V$1.5 multiprotein complex, where the integrin functions as a molecular hub triggering a novel pro-migratory signaling pathway in TNBC cells further stress the relevance of these structures in cancer progression.

The hERG1 potassium and the neonatal Na$_V$ 1.5 sodium channels are co-translated and functionally cooperate in TNBCa

Another relevant finding emerging from the present paper is the fact that the two channels present in the β1 integrin-centered complex in BCa cells, hERG1 and nNa$_V$1.5 are also expressed in the heart (Santini & Duranti et al, 2023). What is more, a functional interplay between the two channels occurs in shaping the cardiac action potential through the association of the two channel proteins during

protein translation. This hERG1/$Na_V1.5$ “microtranslatomes” contribute to coordinate the expression levels of the two currents in the heart (Eichel et al, 2019, Jameson et al, 2023). This is in line with our data from BCa cells either silenced for the two ion channels (or treated with their specific blockers) or transfected with hERG1. In particular, we showed that overexpressing hERG1 also increases $nNa_V1.5$ expression, both at the mRNA, protein and current levels, suggesting that the two channels are likely to be present at similar levels in BCa cells to ensure proper regulation of key cancer cell processes, such as migration and invasion.

Interestingly, through a correlation analysis of *in silico* data we showed that a correlation between *KCNH2* and *SCN5A* was present at the RNA level only in BCa while in healthy breast not even a trend was highlighted. This observation is particularly interestingly since it suggests that the co-expression of the two genes might be relevant for their contemporary function within a precise interval of expression (Lastraioli et al, personal communication).

In conclusion, we uncovered a plasma membrane complex that recruits different ion transport proteins that regulate K^+, Na^+ and H^+ fluxes and cooperate in modulating downstream signals and thus malignant behavior. Given its expression also in primary BCa samples, this complex could be targeted to develop novel therapeutic strategies for one of the most difficult-to-treat cancers, i.e. TNBCa.

MATERIALS AND METHODS

Cell culture and transfection. The MDA-MB-231, MDA-MB-468, MCF-7 and SKBR3 cell lines were cultured in Dulbecco's modified eagle medium (DMEM) with 2% L-glutamine and foetal bovine serum (5% for the MDAs cell lines, 10% for MCF-7 and SKBR3). MDA-MB-231 cells stably transfected with hERG1 were cultured in Dulbecco's modified eagle medium (DMEM) with 2% L-glutamine, 5% foetal calf serum. EBNA cells stably transfected with adult $Na_V1.5$ ($aNa_V1.5$) and $nNa_V1.5$ were cultured in DMEM (Euroclone, Milan, Italy) with 2% L-Glutamine, 10% fetal calf serum. MDA-MB-231 cells stably transfected with hERG1 (MDA-MB-231-T) and with the empty vector were cultured in DMEM with 2% L-glutamine (Euroclone), 5% fetal calf serum (Euroclone, Milan, Italy) and 2 mg/ml geneticin (G418) (Thermo Fisher Scientific, Waltham, MA). Cells were routinely cultured at 37 °C with 5% CO2 in a humidified atmosphere.

Gene silencing experiments. For gene silencing experiments, cells were cultured as above in 60mm cell culture plates (Corning Costar; Corning, NY, USA). Twenty-four hours after plating cells were transfected with two different KCNH2-siRNAs (44858 anti-hERG1 siRNA1 and 44762 anti-hERG1 siRNA2; Ambion; Austin, TX, USA); β1 integrin siRNA (109878 ITGB1; Invitrogen, Waltham, USA) and custom made SCN5A-siRNAs (siNESO1 and siNESO2). A control transfection was also carried out using scrambled siRNAs. The final concentration of the siRNAs was 100 nM in Lipofectamine 2000 reagent (Invitrogen; Carlsbad CA, USA). Transfection followed the manufacturer's instructions. After 5 hours, the medium was changed and, after overnight incubation, 1 ml Optimem (Gibco; Carlsbad CA, USA) was added. Selection and further cell culture were performed in complete culture medium supplemented with 2.0 mg/ml geneticin (G418). Twenty-four hours later, the supernatant and cells were collected for RNA extraction (see below). 48 hours after transfection, cells were collected, and RNA processed. The siRNA-transfected cells are referred to as

"MDA-MB-231-T". A control transfection was also carried out using scrambled siRNA. The latter are referred to as "MDA-MB-231" since they were identical to MDA-MB-231 un-transfected cells.

RNA extraction, reverse transcription and real-time quantitative PCR. RNA extraction and reverse transcription were performed as previously described (Pillozzi et al, 2007). It involved the following primers: neonatal-*SCN5A (nSCN5A)* - 5-CTGCACGCGTTCACTTTCCT-3' (forward) / 5'-GACAAATTGCCTAGTTTTATATTT-3' (reverse) ; adult-*SCN5A* (*aSCN5A*) - 5′-CTGCACGCGTTCACTTTCCT-3′ (forward) / 5′-CAGCCAGCTTCTTCACAGACT-3′ (reverse); *KCNH2* - 5'-GAGTACAGCCGCTGGATG-3' (forward) / 5'-ACGTCTCTCCCAACACCA-3' (reverse). The SYBR Green fluorescent dye (Power SYBR Green PCR Master Mix, Applied Biosystems; Waltham, MA, USA) protocol was used. Glyceraldehyde-3-phosphate dehydrogenase gene was used as a standard reference: *GADPH*: (forward) 5'-ACGACCAAATCCGTTGACTC-3' / (reverse) 5'-GCTGTCTGCTCCTCCTGTTC-3'. Calibration was performed using HEK-293 and HEK-hERG1 cell lines for *KCNH2* and EBNA-nNa$_V$1.5 for nNa$_V$1.5. ΔΔCt method was used for the relative quantification of the expression levels. Amplification of a specific products or primer–dimer artefacts was excluded by melting curve analysis. Each reaction was performed in triplicate.

Preparation of cells for experiments. For all experiments, excluding Matrigel invasion assay, all the cell types were starved overnight by culturing them in serum-free-BSA medium, containing 250 mg/ml of heat inactivated (HI) BSA (Fraction V, Euroclone, Milan, Italy). The day after, cells were harvested by detaching them with 5 mM EDTA in phosphate-buffered saline (PBS) (Euroclone, Milan, Italy) and resuspended in serum-free medium. Next, cells were seeded on FN-coated dishes/slides. To this purpose culture dishes/glass slides were first coated with fibronectin (Sigma-Aldrich, Darmstadt, Germany, human plasma) at 5 μg/cm^2 concentration diluted in sterile PBS. The dishes were left air-drying for 1 h at room temperature before introducing cells and medium. Hence, cells detached and resuspended in serum-free-BSA medium, were added at different concentrations depending on the type of experiment to be performed. For experiments with silenced cells the overnight starvation was not carried out.

Treatments. We used the following inhibitors: 40 µM E4031 (Tocris, Bristol, UK; hERG1 blocker; Masi et al, 2005); 20µM tetrodotoxin (TTX) (Tocris, Bristol, UK; $nNa_V1.5$ blocker; Guzel et al, 2019, 20µg/ml scDb-hERG1-β1 (MCK Therapeutics Srl, Pistoia, Italy; hERG1/β1 integrin complex blocker; Duranti et al, 2021; Duranti and Iorio et al, 2023) and 5 µM cariporide (Tocris, Bristol, UK; specific NHE1 inhibitor; Hulikova et al, 2013).

Protein extraction, co-immunoprecipitation and Western Blotting. Cells were starved O/N in culture media plus heat-inactivated BSA (250 mg/ml; Fraction V). Cells were harvested by detaching with 5 mM EDTA in phosphate-buffered saline (PBS) and resuspended in culture media plus heat-inactivated BSA were seeded onto dishes pre-coated with 5 µg/cm^2 fibronectin (in sterile PBS). For (co)-immunoprecipitation experiments, cells were seeded and incubated on fibronectin for 120 minutes. Protein extraction, quantification and total lysate incubation with protein A/G agarose beads (Santa Cruz Biotechnology; Dallas, TX, USA) were performed as reported by Becchetti et al, (2017). Protein extraction, quantification and total lysate incubation with protein A/G agarose beads (Santa Cruz Biotechnology; Dallas, TX, USA) were performed as reported by Becchetti et al, 2017. The composition of the lysis buffer was the following: NP40 (150 mM), NaCl (150 mM), Tris-HCl pH 8 (50 mM), EDTA pH 8 (5 mM), NaF (10 mM), $Na_4P_2O_7$ (10 mM), Na_3VO_4 (0.4 mM), and a protease inhibitor cocktail (complete Mini, Roche; Basel, Switzerland). The TS2/16 antibody (details are reported in Table S1) was used to immunoprecipitate β1-integrin; the mAb-hERG1 antibody (details are reported in Table S1) was used to immunoprecipitate hERG1 protein. The Clone TS2/16 antibody was left incubating overnight and after that the immuno-complex was captured by adding 50µl of protein A/G agarose (Merck Sigma, Burlington, MA) beads for 2 hours at 4°C (with rolling agitation). The incubation was followed by two washing steps: 3 times with ice-cold wash buffer and 3 times with ice-cold PBS. Then, 10µl of 2X Laemmli Buffer were added and the proteins were boiled for 5 min at 95°C. SDS-PAGE was performed and following electrophoresis, proteins were transferred onto PVDF membrane (previously activated) in blotting buffer at 4°C for 1 h at 150 V. 5% BSA in T-PBS (0.1% tween, Merck Sigma, Burlington, MA) solution was then used to block the PVDF

membrane, for 3 hours at room temperature (this step is required to cover the unspecific antibody binding sites on the membrane). Blots were then incubated overnight at 4°C with primary antibodies (type and antibodies dilution are described in Table S1). The following day the membrane was washed with T-PBS (0.1% tween) (15 min x 3 times) and appropriate secondary antibody: (i) anti-rabbit antibody conjugated with peroxidase enzyme (Merck Sigma, Burlington, MA) was dissolved in 5% BSA in T-PBS (0.1% tween) (dilution 1:10.000) for at least 45 min and washed (15 min x 3 times), revealing was performed using ECL solution (Amersham, Buckinghamshire, UK) for anti-C54 primary antibody and (ii) for all other primary antibodies, IRDYe 800 CW anti-mouse or anti-rabbit antibody (LI-COR Biosciences, Nebraska, USA) was dissolved in 5% BSA in T-PBS (0.1% tween) (dilution 1:20.000) for at least 45 min and washed (15 min x 3 times) before membrane scanning using LI-COR Odyssey (Biosciences, Nebraska, USA).

Densitometric analysis. Co-immunoprecipitated hERG1, β1 integrin, NHE1 and $nNa_V1.5$ proteins, alone and in combination, were quantified by optical densitometry. The co-immunoprecipitated signal (i.e. hERG1) was first separated by the signal of the protein used for the immunoprecipitation process (i.e. β1 integrin) and then normalized to the signal of the corresponding protein obtained in the total lysate (i.e. hERG1). ImageJ was used to analyze data and graphs were plotted using OriginPro8 software (OriginLab Corporation; Northampton, MA, USA). The expression levels of the proteins in WB and co-IP have been quantified as reported above. Then they have been normalized as following: (WB quantification/IF quantification)*100.

Immunofluorescence. 24-well plates were prepared with one coverslip pre-coated with Fibronectin 5μg/cm^2 placed in each well and incubated at least 1 hour. Then the coating solution was removed and 2x10^{4}cells were seeded on each coverslip and left to settle for 2h. Cells were then fixed with 500μL 4% paraformaldehyde (PFA) (Thermo scientific, Rockford, IL, USA) solution in PBS 1X, pH 7.4 at room temperature. After 10 minutes, the PFA solution was removed and each well was washed with PBS 3 times (5 minutes each). Cells were then 'blocked' by washing once with 500μl of 10% BSA solution in PBS (pH 7.4), for 1 hour at room temperature. A solution of the primary antibody

Alexa-488 or Alexa-647 conjugated (at final concentration indicated in Table S1) was made up and 100µl were added onto each coverslip placed on a podium in a humidity chamber and cells were allowed to incubate overnight in a cold room (6-7°C) for hERG1 and nNav1.5 staining and 2 hours at room temperature for hERG1/β1 integrin complex labelling. For paxillin and Arp2/3 detection, overnight incubation in a cold room (6-7°C) was carried and anti-mouse/rabbit secondary antibody Alexa-488 conjugated (Thermo Fisher Scientific, Waltham, MA) incubation was performed (1 hour, room temperature, 1.500 final dilution). Then, each coverslip was washed with PBS 3 times each for 5 minutes and nuclei were stained with Hoechst (Merck Sigma, Burlington, MA; 15 min, room temperature, 1:1000 final dilution) and slides were mounted using Prolong Diamond antifade mountant (Invitrogen, Waltham, Massachusets, USA). To investigate cytoskeletal actin architecture using confocal microscopy, cells were fixed using 4% PFA, followed by permeabilization (0.1% Triton-X; Merck Sigma, Burlington, MA), blocking with 1% BSA and staining with rhodamine-conjugated phalloidin following manufacturer's instructions (Invitrogen, Waltham, MA, USA) and Hoechst (15 min, room temperature, 1:1000 final dilution) and slides were mounted using Prolong Diamond antifade mountant (Invitrogen, Waltham, Massachusets, USA). Pictures were taken on a confocal microscope (Nikon TE2000, Nikon; Minato, Tokyo, Japan).

Immunofluorescence signal quantification. In all immunofluorescence experiments, the fluorescence relative to 20 cells (in 10 different fields and 3 different experiments) per each condition was determined using ImageJ Software. For total IF signal, we measured the mean fluorescence intensity for each cell. When needed, the fluorescent intensity at the plasma membrane level was quantified considering exclusively the signals arising at the periphery of the cells. To this purpose we draw a mask (highlighted by white circular lines in the figures) that was performed determined using the "freeform line profile" function drawn around the cell surface that enucleates only the fluorescent signal related to the membrane which was subsequently quantified using ImageJ Software (Duranti and Iorio et al, 2023). Colocalization was quantified using Manders' Overlap coefficient, which was measured using the Co-loc plugin (Fiji Software) for each cell analyzed. To analyze filopodia, actin

filaments within 2 μm of the cell border were taken into account. The (linear) density of filopodia was calculated as the total number of filopodia normalized by the cell perimeter length. The cortactin staining was quantified as the "Invadopodia Index" (InvI), i.e. percentage of cells showing clear brightly stained spots. $InvI(\%) = \frac{Ns}{Ntot} \times 100$

Ns = cells showing invadopodia spots

Ntot = total number of cells.

Cell proliferation. The 3-(4,5-dimethylthiazo1-2-yl)-2,5-diphenyltetrazolium bromide (MTT) (Merck Sigma, Burlington, MA) reduction assay was used to quantify cell proliferation. The assay enables determination of the level of metabolic activity in eukaryotic cells via cytoplasmic and mitochondrial reduction of MTT (yellow) into formazan crystals (blue). Cells were plated in 24 well plates at a density of $2x10^4$ cells/well and let them settle overnight. The DMEM solution was then replaced with 1mL of treatment solution for 24 hours. Cells were then treated with 100μl of MTT and 400μl of DMEM and incubated (in darkness) for 3 hours as normal at 37°C. The MTT solution was replaced with 50μl of DMSO (Merck Sigma, Burlington, MA). Then, the plates were placed on a rocker in darkness for 10 minutes. The absorbance of each well was read at 570 nm on a multi-well plate reader. Cell number was deduced from a pre-determined linear calibration curve. The latter was generated by serial dilution of cells (50, 25, 12.5, 6.250, 3.125 and $1.5x10^4$) left to settle for 4 hours before applying the MTT protocol. Each calibration and each drug treatment were repeated at least 3 times.

Lateral motility. Lateral motility was determined using 35 mm dishes and drawing 15 horizontal lines and 3 perpendicular lines on the dish bottom, as in Iorio et al, 2020. Plates were coated with FN (Sigma-Aldrich, Darmstadt, Germany, human plasma) and $5x10^5$ cells were seeded and allowed to attach 5-10 min. Then, a manual scratch was done and the width of the wound was determined (W0). At this time, the different treatments were added. Then, dishes were incubated for further for 120 min. At the end of incubation, the width of the wounds (Wt) was determined on unfixed cells. We

took care to do these measurements within non more than 30 min overall. Motility Index (MI) was assessed using the following formula: MI = 1 – Wt/W0, where Wt is the width of the wounds.

Matrigel invasion. Following 24h pre-treatment, cells were plated in 24-well plates containing Transwell® filters (Beckton Dickinson; Oxford, UK) with 8μm pores. Filters were coated a day earlier with 50μL Matrigel® (Beckton Dickinson; Oxford, UK) diluted with FBS-free DMEM to 1.25 mg/mL from a 10 mg/mL stock and left to solidify overnight. Inserts were then hydrated with 0.5mL FBS-free DMEM for 2-3 hours at 37°C. Cells were plated onto the coated filters at a density of $2x10^4$ cells/insert; a chemotactic gradient was produced by adding 300μL of 5% FBS supplemented solutions in the lower chamber and 300μL of 1% FBS supplemented solution in the upper chamber. Treatment with E4031, TTX or E4031+TTX was continued by adding the agent to the upper chamber and cells were allowed to invade for 18 hours. All the solutions were removed and the upper parts of the inserts were swabbed to remove the non-invaded cells. Invaded cells were fixed in 300μL ice-cold methanol (100%) for 15 minutes. Staining was with 200μL of 0.5 g/ml crystal violet in 25% methanol for 15 minutes at room temperature. Inserts were washed with distilled water and dried; stained cells were counted in at least 12 random fields of view/insert at 40x magnification on an inverted microscope. The number of cells counted in each field of view was converted to "cells per mm^2" by multiplying the number of counted cells by a factor of 4.07. For all experiments, a background level of invasion was calculated, seeding the cells without chemotactic gradient, and a basal level of invasion was then subtracted from the measurements.

Electrophysiology. On the experimental day, MDA-MB-231-T and WT cells were detached, resuspended in DMEM 5% FBS with and without 2 mg/ml G418, respectively, and seeded on 35 mm Petri dishes. Electrophysiological recordings were performed at room temperature (~25 °C) in the whole-cell configuration of the patch clamp technique, after 2 h during which cells were maintained in an incubator at 37 °C, 5% CO_2. The patch pipettes were pulled from borosilicate glass capillary tubes to a resistance of 3.5–5 MΩ. Capacitances were manually compensated after the reaching of a stable gigaseal. Experimental protocols and data acquisition were performed with the Multiclamp 700

A or Multiclamp 1D amplifiers and pCLAMP 9.2 software (Molecular Devices, Sunnyvale, CA, USA) was used for data analysis. The hERG1 inward tail currents were recorded with a 25 kHz sampling rate and a 0.2 kHz low-pass filter. Cells' identification and patch were performed at 40× magnification with a Nikon Eclipse TE300 microscope (Nikon Instruments Inc., Amstelveen, The Netherlands), equipped with a Photometrics CoolSNAP CF camera (Teledyne Photometrics, Tucson, AZ, USA). Cell membrane potentials were held at −80 mV, and hERG1 inward tail currents were elicited using preconditioning holding potential from 0 mV to -100 mV (10 mV step increment) followed by 1s hyperpolarizing step (−120 mV) with an intersweep interval of 15 s. The internal pipette solution for hERG1 current recordings contained (in mM): 130 K^+ aspartate, 10 NaCl, 4 $CaCl_2$, 2 $MgCl_2$, 10 Hepes, 10 EGTA, pH 7.3. The external solution contained (in mM): 130 NaCl, 5 KCl, 2 $CaCl_2$, 2 $MgCl_2$, 10 HEPES, 5 glucose (EK = −80 mV), pH of 7.4. IhERG1 amplitude, normalized to the maximum current amplitude, was used to construct the activation curve. The half-maximum activation voltage ($V_{1/2}$) was calculated by fitting I/V curve with Boltzmann function. For Nav1.5 current recordings, the external solution contained (in mM): 144 NaCl, 5.4 KCl, 1 $MgCl_2$, 2.5 $CaCl_2$, 5 HEPES, and 5.6 glucose, pH of 7.3. The pipette solution, instead, contained (in mM): 145 CsCl, 5 NaCl, 2 MgCl2, 11 EGTA, and 10 HEPES, pH of 7.4. Signals were filtered at 5 kHz with a low-pass filter and sampled at 10 kHz. Nav1.5 currents were elicited using preconditioning holding potential from -100 mV to +45 mV (5 mV step increment) with an intersweep interval of 2 s. Resting membrane potential values for all the cell lines were measured in I = 0 mode.

Calcium imaging. The following procedure was performed in the Laboratory of Cellular and Molecular Angiogenesis, Department of Life Sciences and Systems Biology, University of Turin according to a published protocol (Scarpellino et al, 2019). Cells were grown on glass fibronectin- or BSA-coated coverslips, after overnight starvation, at a density of 5000 cells/cm^2 for 2 h. Following that cells were loaded (40 min at 37°C) with 2 µM Fura-2AM (Invitrogen; Carlsbad, CA, USA), for ratiometric cytosolic Ca^{2+} [Ca^{2+}]c measurements. Nikon Eclipse TE-2000S (Nikon; Minato, Tokyo, Japan) inverted microscope was used to acquire fluorescence. [Ca^{2+}]c was expressed as a ratio ® of

emitted fluorescence at 510 nm corresponding to excitation wavelengths of 340 nm and 380 nm. Image acquisition (3 s frequency) was performed using Metafluor Imaging System (Molecular Devices; Sunnyvale, CA, USA). For each experiment, several regions of interest (ROIs) have been selected corresponding to single cells in a chosen image field. Real time background subtraction was applied in order to limit noise. Calcium imaging analysis and quantification (peak amplitude, area, rise time, decay time) were performed using Clampfit software (Axon Pclamp, Molecular Devices; San Jose, CA, USA) and analyzed with GraphPad Prism 8 (GraphPad Software Inc., La Jolla, CA, USA). Area underlying calcium influx during the sustained phase in the presence of extracellular Ca^{2+} was evaluated at 200 s after the onset of the response. Total area under calcium spikes in 0 Caout was measured by the use of Event Detection protocol in Clampfit software.

Measurement of pH_i. To determine pH_i, we used 2',7'-Bis (2-carboxyethyl)-5 (6)-carboxyfluorescein acetoxymethyl ester (BCECF-AM) (Sigma-Aldrich, Darmstadt, Germany). Cells were starved overnight. After starvation, 50.000 cells were seeded in no-serum medium onto BSA or FN coated surfaces of 96-well plates (clear bottom 96-well plate, polystyrene, TC-treated, clear flat bottom wells, sterile, w/lid, black; Corning, New York, USA) and incubated at 37°C and 5% CO_2 for 2 h, in the absence or presence of different treatments. At 2 h, the medium was removed and BCECF-AM (1μM final concentration in loading solution (HBSS 1X (Euroclone, Milan, Italy) plus 0.01% $NaHCO_3$, pH 7.4)) was added for 30 min at 37°C and 5% CO_2. After incubation, cells were washed twice with loading solution at room temperature. The time zero pH_i (T_0) was measured in detached cells, before seeding, at room temperature. The pH_i of detached cells was determined in 96-well plate with microplate reader and the appropriate standard curve. Fluorescence intensity was immediately measured with a microplate reader at the following wavelengths: 440–490nm for excitation and 535 nm for emission. A calibration curve was set up using a high K^+/Nigericin solution (135 mM KCl, 2 mM K_2HPO_4, 20 mM HEPES, 1.2 mM $CaCl_2$ and 0.8 mM $MgSO_4$), in a range of pH from 5.0 to 8.5. All pH values were calculated using 490/440nm fluorescence ratio and applying standard curve and linear equations.

Statistical analysis. Unless otherwise indicated, data are given as mean values ± SEM, with n indicating the number of independent experiments. Statistical comparisons were performed with OriginPro 2015 and SAS 9.2 (SAS Institute) software. The normality of data distribution was checked with K-S test. In the case of normal distributions, each data set was first checked for variance homogeneity, using the F test for equality of two variances and the Brown-Forsythe test for multiple comparisons. For data with unequal variances, the Welch correction was applied. For comparisons between two groups of data, we used the Student's t test. A two-sample K-S test was performed to test whether two underlying probability distributions differed. For multiple comparisons, one-way ANOVA followed by Bonferroni's post hoc test was performed to derive P values. As reported in the figure legends, in case of unequal variances, ANOVA was followed by the Hochberg's GT2 post hoc method. In the case of nonnormal distributions, nonparametric Kruskal-Wallis ANOVA followed by DSCF's post hoc method was applied. The relevant P values are reported in the figure panels and legends. The Pearson coefficient (R) was calculated to evaluate relationships between continuous variables ($R = -1$ negative relationship; $R = 0$ no relationship; $R = 1$ positive relationship).

ACKNOWLEDGMENTS

The authors thank Dr Matteo Lulli for confocal microscopy, (Department of Experimental and Clinical Biochemical Sciences, Section of General Pathology, University of Florence , Florence, Italy); Prof Luca Munaron and Prof Alessandra Fiorio Pla for help in experiments measuring intracellular Ca^{2+} (Department of Life Sciences and Systems Biology, University of Torino, via Accademia Albertina 13, 10123 Torino, Italy).

AUTHOR CONTRIBUTION

C.C. and J.I. Formal analysis, supervision, investigation, visualization, methodology, writing–original draft; E.L. Formal analysis, investigation, visualization, methodology, writing–original draft; C.D. Formal analysis, investigation, visualization, methodology; G.B., G.C.A., R.C. and G.S. Investigation, methodology; S.P.F. Conceptualization, writing–original draft; M.B.A.D. Conceptualization, supervision, writing–original draft; A.B. Conceptualization, supervision; A.A. Conceptualization, formal analysis, supervision, funding acquisition, investigation, visualization, methodology, writing–original draft, project administration.

FUNDINGS

This research was funded by the University of Florence (ex 60%) to A Arcangeli. This work was supported by Associazione Italiana per la Ricerca sul Cancro (AIRC, grant nos. 1662, 15627, and 21510) to A Arcangeli, PRIN Italian Ministry of University and Research (MIUR) “Leveraging basic knowledge of ion channel network in cancer for innovative therapeutic strategies (LIONESS)” 20174TB8KW and “Dynamics of ion channel-based macromolecular complexes in triggering mechanotransduction through lipid rafts: towards understanding mechanisms underlying cell invasiveness in pancreatic cancer (MECHIONRAFT)” 2022APEBMY to A Arcangeli, pHioniC: European Union’s Horizon 2020 grant No 813834 to A Arcangeli. The data presented in the current study were in part generated using grants by the European Union - NextGenerationEU - National

Recovery and Resilience Plan, Mission 4 Component 2 - Investment 1.5 - THE - Tuscany Health Ecosystem - ECS00000017 - CUP B83C22003920001 to C Duranti and A Arcangeli. The data presented in the current study were in part generated using grants by European Union, National Recovery and Resilience Plan, Mission 4 Component 2 – Investment 1.4 - National Center for Gene Therapy and Drugs based on RNA Technology - NextGenerationEU – Project Code CN00000041- CUP B13C22001010001 to A Arcangeli. J Iorio was supported by Regione Toscana fellowship within the project "Progetti di alta formazione attraverso l'attivazione di Assegni di Ricerca" (MutCoP project) co-funded by Fondazione Cassa di Risparmio di Pistoia e Pescia and was formerly funded by a fellowship of Fondazione Cassa di Risparmio di Pistoia e Pescia within Giovani@Ricerca Scientifica program. This work was also supported by the University of Milano-Bicocca to A Becchetti (grant 2021-ATE-0042). C Duranti was supported by an AIRC fellowship for Italy "Francesco Tonni" ID 24020.

REFERENCES

Alghanem AF, Abello J, Maurer JM, Kumar A, Ta CM, Gunasekar SK, Fatima U, Kang C, Xie L, Adeola O, Riker M, Elliot-Hudson M, Minerath RA, Grueter CE, Mullins RF, Stratman AN, Sah R. 2021. The SWELL1-LRRC8 complex regulates endothelial AKT-eNOS signaling and vascular function. *Elife*.**10**:e61313. doi: 10.7554/eLife.61313.

Arcangeli A, Duranti C, Iorio J, Lastraioli E. 2023. The role of potassium channels in tumours of the gastrointestinal tract: a focus on the human ether-à-go-go related gene 1 channels. *J Physiol*. **601(9):**1597-1610. doi: 10.1113/JP282310.

Arcangeli A, Iorio J, Duranti C. 2024. Targeting the hERG1 and β1 integrin complex for cancer treatment. *Expert Opin Ther Targets*. **1-13**. doi: 10.1080/14728222.2024.2318449.

Artym VV, Petty HR. 2002. Molecular proximity of Kv1.3 voltage-gated potassium channels and β1-integrins on the plasma membrane of melanoma cells: effects of cell adherence and channel blockers. *J Gen Physiol* **120**:29–37. doi:10.1085/jgp.20028607.

Ashburner M, Ball CA, Blake JA, Botstein D, Butler H, Cherry JM, Davis AP, Dolinski K, Dwight SS, Eppig JT, Harris MA, Hill DP, Issel-Tarver L, Kasarskis A, Lewis S, Matese JC, Richardson JE, Ringwald M, Rubin GM, Sherlock G. Gene ontology: tool for the unification of biology. The Gene Ontology Consortium. 2000. *Nat Genet*. **25**(1):25-9. doi: 10.1038/75556.

Badaoui M, Mimsy-Julienne C, Saby C, Van Gulick L, Peretti M, Jeannesson P, Morjani H, Ouadid-Ahidouch H. 2018. Collagen type 1 promotes survival of human breast cancer cells by overexpressing Kv10.1 potassium and Orai1 calcium channels through DDR1-dependent pathway. *Oncotarget* **9**:24653–24671. doi:10.18632/oncotarget.19065.

Baroni D, Picco C, Moran O. 2017. Mutation E87Q of the β1-subunit impairs the maturation of the cardiac voltage-dependent sodium channel. *Sci Rep* **7**:10683. doi:10.1038/s41598-017-10645-y.

Becchetti A, Crescioli S, Zanieri F, Petroni G, Mercatelli R, Coppola S, Gasparoli L, D'Amico M, Pillozzi S, Crociani O, Stefanini M, Fiore A, Carraresi L, Morello V, Manoli S, Brizzi MF, Ricci D, Rinaldi M, Masi A, Schmidt T, Quercioli F, Defilippi P, Arcangeli A. 2017. The conformational state

of hERG1 channels determines integrin association, downstream signaling, and cancer progression. *Sci Signal* **10**:eaaf3236. doi:10.1126/SCISIGNAL.AAF3236.

Becchetti A, Duranti C, Arcangeli A. 2022. Dynamics and physiological meaning of complexes between ion channels and integrin receptors: the case of Kv11.1. *Am J Physiol Cell Physiol* **322**:C1138–C1150. doi:10.1152/ajpcell.00107.2022.

Becchetti A, Petroni G, Arcangeli A. 2019. Ion Channel Conformations Regulate Integrin-Dependent Signaling. *Trends Cell Biol*. **29(4)**:298-307. doi: 10.1016/j.tcb.2018.12.005.

Beckham Y, Vasquez RJ, Stricker J, Sayegh K, Campillo C, Gardel ML. 2014. Arp2/3 inhibition induces amoeboid-like protrusions in MCF10A epithelial cells by reduced cytoskeletal-membrane coupling and focal adhesion assembly. *PLoS One* **9**(6):e100943. doi:10.1371/journal.pone.0100943.

Brackenbury WJ, Chioni AM, Diss JKJ, Djamgoz MBA. 2007. The neonatal splice variant of Nav1.5 potentiates in vitro invasive behaviour of MDA-MB-231 human breast cancer cells. *Breast Cancer Res Treat* **101**:149–160. doi:10.1007/s10549-006-9281-1.

Breuer EK, Fukushiro-Lopes D, Dalheim A, Burnette M, Zartman J, Kaja S, Wells C, Campo L, Curtis KJ, Romero-Moreno R, Littlepage LE, Niebur GL, Hoskins K, Nishimura MI, Gentile S. 2019. Potassium channel activity controls breast cancer metastasis by affecting β-catenin signaling. Cell Death Dis. **10**(3):180. doi: 10.1038/s41419-019-1429-0.

Brisson L, Driffort V, Benoist L, Poet M, Counillon L, Antelmi E, Rubino R, Besson P, Labbal F, Chevalier S, Reshkin SJ, Gore J, Roger S. 2013. NaV1.5 Na^+ channels allosterically regulate the NHE-1 exchanger and promote the activity of breast cancer cell invadopodia. *J Cell Sci* **126**:4835–4842. doi:10.1242/jcs.123901.

Brisson L, Gillet L, Calaghan S, Besson P, Le Guennec JY, Roger S, Gore J. 2011. Na v 1.5 enhances breast cancer cell invasiveness by increasing NHE1-dependent H efflux in caveolae. *Oncogene* **30**: 2070–2076. doi:10.1038/onc.2010.574.

Cherubini A, Hofmann G, Pillozzi S, Guasti L, Crociani O, Cilia E, Balzi M, Degani S, Di Stefano P, Defilippi P, Wanke E, Becchetti A, Olivotto M, Wymore R, Arcangeli A. 2005 Human ether-a-go-

go-related gene 1 channels are physically linked to β1 integrins and modulate adhesion-dependent signaling. *Mol Biol Cell* **16**:2972–2983. doi:10.1091/mbc.e04-10-0940.

Cherubini A, Pillozzi S, Hofmann G, Crociani O, Guasti L, Lastraioli E, Polvani S, Masi A, Becchetti A, Wanke E, Olivotto M, Arcangeli A. 2002. $K_V11.1$ K^+ channels and β1 integrins interact through the assembly of a macromolecular complex. *Ann N Y Acad Sci* **973**:559–561. doi:10.1111/j.1749-6632.2002.tb04701.x.

Chioccioli Altadonna G, Montalbano A, Iorio J, Becchetti A, Arcangeli A, Duranti C. 2022. The Interaction between hERG1 and β1 Integrins Modulates hERG1 Current in Different Pathological Cell Models. *Membranes (Basel)* **12**:1162. doi:10.3390/MEMBRANES12111162.

Condeelis J, Vahey M. 1982. A calcium- and pH-regulated protein from Dictyostelium discoideum that cross-links actin filaments. *J Cell Biol.* **94**(2):466-71. doi: 10.1083/jcb.94.2.466. PMID: 7107709; PMCID: PMC2112894.

Contois L, Akalu A, Brooks PC. 2009. Integrins as "functional hubs" in the regulation of pathological angiogenesis. *Semin Cancer Biol* **19**:318-28. doi:10.1016/j.semcancer.2009.05.002.

Denker SP, Barber DL. 2002. Ion transport proteins anchor and regulate the cytoskeleton. *Curr Opin Cell Biol.* **14(2)**:214-20. doi: 10.1016/s0955-0674(02)00304-6.

Dufort CC, Paszek MJ, Weaver VM. 2011. Balancing forces: Architectural control of mechanotransduction. *Nat Rev Mol Cell Biol* **12**:308–319. doi:10.1038/nrm3112.

Duranti C, Iorio J, Bagni G, Chioccioli Altadonna G, Fillion T, Lulli M, D'Alessandro FN, Montalbano A, Lastraioli E, Fanelli D, Coppola S, Schmidt T, Piazza F, Becchetti A, Arcangeli A. 2023. Integrins regulate hERG1 dynamics by girdin-dependent Gαi3: signaling and modeling in cancer cells. *Life Sci Alliance*. **7(1)**:e202302135. doi: 10.26508/lsa.202302135.

Duranti C, Iorio J, Lottini T, Lastraioli E, Crescioli S, Bagni G, Lulli M, Capitani C, Bouazzi R, Stefanini M, Carraresi L, Iamele L, De Jonge H, Arcangeli A. 2021. Harnessing the hERG1/β1 Integrin Complex via a Novel Bispecific Single-chain Antibody: An Effective Strategy against Solid Cancers. *Mol Cancer Ther* **20**:1338-1349. doi:10.1158/1535-7163.

Eichel CA, Ríos-Pérez EB, Liu F, Jameson MB, Jones DK, Knickelbine JJ, Robertson GA. 2019. A microtranslatome coordinately regulates sodium and potassium currents in the human heart. *Elife* **8**:e52654. doi:10.7554/ELIFE.52654.

Frantz C, Barreiro G, Dominguez L, Chen X, Eddy R, Condeelis J, Kelly MJ, Jacobson MP, Barber DL. 2008. Cofilin is a pH sensor for actin free barbed end formation: role of phosphoinositide binding. *J Cell Biol*. **183**:865-79. doi:10.1083/jcb.200804161.

Fraser SP, Salvador V, Manning EA, Mizal J, Altun S, Raza M, Berridge RJ, Djamgoz MB. 2003 Contribution of functional voltage-gated Na^+ channel expression to cell behaviors involved in the metastatic cascade in rat prostate cancer: I. Lateral motility. *J Cell Physiol* **195**:479–487. doi:10.1002/jcp.10312.

Fraser SP, Diss JK, Chioni AM, Mycielska ME, Pan H, Yamaci RF, Pani F, Siwy Z, Krasowska M, Grzywna Z, Brackenbury WJ, Theodorou D, Koyutürk M, Kaya H, Battaloglu E, De Bella MT, Slade MJ, Tolhurst R, Palmieri C, Jiang J, Latchman DS, Coombes RC, Djamgoz MB. 2005. Voltage-gated sodium channel expression and potentiation of human breast cancer metastasis. *Clin Cancer Res* **11**:5381–5389. doi:10.1158/1078-0432.CCR-05-0327.

Fukushiro-Lopes DF, Hegel AD, Rao V, Wyatt D, Baker A, Breuer EK, Osipo C, Zartman JJ, Burnette M, Kaja S, Kouzoukas D, Burris S, Jones WK, Gentile S. 2017. Preclinical study of a Kv11.1 potassium channel activator as antineoplastic approach for breast cancer. *Oncotarget.* **9**(3):3321-3337. doi: 10.18632/oncotarget.22925.

Gardel ML, Schneider IC, Aratyn-Schaus Y, Waterman CM. 2010. Mechanical integration of actin and adhesion dynamics in cell migration. *Annu Rev Cell Dev Biol* **26**:315–333. doi:10.1146/annurev.cellbio.011209.122036

Gillet L, Roger S, Besson P, Lecaille F, Gore J, Bougnoux P, Lalmanach G, Le Guennec JY. 2009. Voltage-gated Sodium Channel Activity Promotes Cysteine Cathepsin-dependent Invasiveness and Colony Growth of Human Cancer Cells. *J Biol Chem*. **284**(13):8680-91. doi: 10.1074/jbc.M806891200.

Goldman MJ, Craft B, Hastie M, Repečka K, McDade F, Kamath A, Banerjee A, Luo Y, Rogers D, Brooks AN, Zhu J, Haussler D. 2020. Visualizing and interpreting cancer genomics data via the Xena platform. *Nat Biotechnol*. **38**(6):675-678. doi: 10.1038/s41587-020-0546-8.

Gunasekar SK, Xie L, Sah R. 2019. SWELL signalling in adipocytes: can fat 'feel' fat? *Adipocyte*. **8**(1):223-228. doi: 10.1080/21623945.2019.1612223.

Guzel RM, Ogmen K, Ilieva KM, Fraser SP, Djamgoz MBA. 2019. Colorectal cancer invasiveness in vitro: Predominant contribution of neonatal Nav1.5 under normoxia and hypoxia. *J Cell Physiol*. **234**(5):6582-6593. doi: 10.1002/jcp.27399.

Hanahan D, Weinberg RA. 2011. Hallmarks of cancer: the next generation. *Cell* **144:**646–674. doi:10.1016/j.cell.2011.02.013.

Heijman J, Dobrev D. 2018. Ion channels as part of macromolecular multiprotein complexes: Clinical significance. *Herzschrittmacherther Elektrophysiol* **29**:30–35. doi:10.1007/s00399-017-0542-y.

Hynes RO, Lively JC, McCarty JH, Taverna D, Francis SE, Hodivala-Dilke K, Xiao Q. 2002. The diverse roles of integrins and their ligands in angiogenesis. *Cold Spring Harb Symp Quant Biol*. **67**:143-53. doi: 10.1101/sqb.2002.67.143.

Hodgkin AL, Huxley AF. 1990. A quantitative description of membrane current and its application to conduction and excitation in nerve. 1952. *Bull Math Biol* **52**:25–71. doi:10.1007/BF02459568.

Ibata N, Terentjev EM. 2020. Development of Nascent Focal Adhesions in Spreading Cells. *Biophys J* **119**:2063–2073. doi:10.1016/j.bpj.2020.09.037.

Hulikova A, Harris AL, Vaughan-Jones RD, Swietach P. 2013. Regulation of intracellular pH in cancer cell lines under normoxia and hypoxia. *J. Cell Physiol*. **228**:743–752. doi: 10.1002/jcp.24221.

Iorio J, Antonuzzo L, Scarpi E, D'Amico M, Duranti C, Messerini L, Sparano C, Caputo D, Lavacchi D, Borzomati D, Antonelli A, Nibid L, Perrone G, Coppola A, Coppola R, di Costanzo F, Lastraioli E, Arcangeli A. 2022. Prognostic role of hERG1 Potassium Channels in Neuroendocrine Tumours of the Ileum and Pancreas. *Int J Mol Sci.* **23(18):**10623. doi: 10.3390/ijms231810623.

Iorio J, Duranti C, Lottini T, Lastraioli E, Bagni G, Becchetti A, Arcangeli A. 2020. $K_V11.1$

Potassium Channel and the Na^+/H^+ Antiporter NHE1 Modulate Adhesion-Dependent Intracellular pH in Colorectal Cancer Cells. *Front Pharmacol* **11**:848. doi:10.3389/fphar.2020.00848.

Iorio J, Meattini I, Bianchi S, Bernini M, Maragna V, Dominici L, Casella D, Vezzosi V, Orzalesi L, Nori J, Livi L, Arcangeli A, Lastraioli E. 2018. hERG1 channel expression associates with molecular subtypes and prognosis in breast cancer. *Cancer Cell Int* **18**:93. doi:10.1186/s12935-018-0592-1.

Jameson MB, Ríos-Pérez EB, Liu F, Eichel CA, Robertson GA. 2023. Pairwise biosynthesis of ion channels stabilizes excitability and mitigates arrhythmias. *Proc Natl Acad Sci U S A*. **120**:e2305295120. doi:10.1073/pnas.2305295120.

Johnston SA, Bramble JP, Yeung CL, Mendes PM, Machesky LM. 2008. Arp2/3 complex activity in filopodia of spreading cells. *BMC Cell Biol* **9**:65. doi:10.1186/1471-2121-9-65.

Jones JL, Walker RA. 1999. Integrins: a role as cell signalling molecules. *Mol Pathol*. **52**:208-13. doi:10.1136/mp.52.4.208.

Kang C, Xie L, Gunasekar SK, Mishra A, Zhang Y, Pai S, Gao Y, Kumar A, Norris AW, Stephens SB, Sah R. 2018. SWELL1 is a glucose sensor regulating β-cell excitability and systemic glycaemia. Nat Commun. **9**(1):367. doi: 10.1038/s41467-017-02664-0.

Kao J, Salari K, Bocanegra M, Choi YL, Girard L, Gandhi J, Kwei KA, Hernandez-Boussard T, Wang P, Gazdar AF, Minna JD, Pollack JR. 2009. Molecular Profiling of Breast Cancer Cell Lines Defines Relevant Models and Provides a Resource for Cancer Gene Discovery. *PLoS One* **4**: e6146. doi:10.1371/journal.pone.0006146.

Kim D, Kim S, Koh H, Yoon SO, Chung AS, Cho KS, Chung J. 2001. Akt/PKB promotes cancer cell invasion via increased motility and metalloproteinase production. *FASEB J*. **15**:1953-62. doi:10.1096/fj.01-0198com.

Koedoot E, Fokkelman M, Rogkoti VM, Smid M, van de Sandt I, de Bont H, Pont C, Klip JE, Wink S, Timmermans MA, Wiemer EAC, Stoilov P, Foekens JA, Le Dévédec SE, Martens JWM, van de Water B. 2019. Uncovering the signaling landscape controlling breast cancer cell migration identifies novel metastasis driver genes. *Nat Commun*. **10**(1):2983. doi: 10.1038/s41467-019-11020-3.

Kovac B, Mäkelä TP, Vallenius T. 2018. Increased α-actinin-1 destabilizes E-cadherin-based adhesions and associates with poor prognosis in basal-like breast cancer. *PLoS One*. **13**(5):e0196986. doi: 10.1371/journal.pone.0196986.

Lachmann A, Xie Z, Ma'ayan A. blitzGSEA: efficient computation of gene set enrichment analysis through gamma distribution approximation. 2022. *Bioinformatics.* **38**(8):2356-2357. doi: 10.1093/bioinformatics/btac076. PMID: 35143610; PMCID: PMC9004650.

Lansu K, Gentile S. 2013. Potassium channel activation inhibits proliferation of breast cancer cells by activating a senescence program. *Cell Death Dis* **4**:e652–e652. doi:10.1038/cddis.2013.174.

Lastraioli E, Iorio J, Arcangeli A. 2015. Ion channel expression as promising cancer biomarker. *Biochim Biophys Acta - Biomembr* **1848**:2685–2702. doi:10.1016/j.bbamem.2014.12.016.

Lee A, Djamgoz MBA. 2018. Triple negative breast cancer: Emerging therapeutic modalities and novel combination therapies. *Cancer Treat Rev* **62**:110–122. doi:10.1016/j.ctrv.2017.11.003.

Levite M, Cahalon L, Peretz A, Hershkoviz R, Sobko A, Ariel A, Desai R, Attali B, Lider O. 2000. Extracellular K+ and opening of voltage-gated potassium channels activate T cell integrin function: physical and functional association between Kv1.3 channels and β1 integrins. *J Exp Med* **191**:1167–1176. doi:10.1084/jem.191.7.1167.

Liu Y, White KA, Barber DL. 2020. Intracellular pH Regulates Cancer and Stem Cell Behaviors: A Protein Dynamics Perspective. *Front Oncol*. **10**:1401. doi: 10.3389/fonc.2020.01401. PMID: 32983969; PMCID: PMC7479815.

Lottini T, Duranti C, Iorio J, Martinelli M, Colasurdo R, D'Alessandro FN, Buonamici M, Coppola S, Devescovi V, La Vaccara V, Coppola A, Coppola R, Lastraioli E, Arcangeli A. 2023. Combination Therapy with a Bispecific Antibody Targeting the hERG1/β1 Integrin Complex and Gemcitabine in Pancreatic Ductal Adenocarcinoma. *Cancers (Basel)* **15:**2013. doi:10.3390/cancers15072013.

Luo Q, Wu T, Wu W, Chen G, Luo X, Jiang L, Tao H, Rong M, Kang S, Deng M. 2020. The Functional Role of Voltage-Gated Sodium Channel $Na_V1.5$ in Metastatic Breast Cancer. *Front Pharmacol* **11**:1111. doi:10.3389/FPHAR.2020.01111.

Manoli S, Coppola S, Duranti C, Lulli M, Magni L, Kuppalu N, Nielsen N, Schmidt T, Schwab A, Becchetti A, Arcangeli A. 2019. The activity of hERG1 potassium channel modulates F-Actin organization during cell migration of pancreatic ductal adenocarcinoma cells. *Cancers (Basel)* **11**:135. doi:10.3390/cancers11020135.

Marques-Carvalho MJ, Oppermann J, Muñoz E, Fernandes AS, Gabant G, Cadene M, Heinemann SH, Schönherr R, Morais-Cabral JH. 2016. Molecular Insights into the Mechanism of Calmodulin Inhibition of the EAG1 Potassium Channel. *Structure* **24**:1742–1754. doi:10.1016/j.str.2016.07.020.

Masi A, Becchetti A, Restano-Cassulini R, Polvani S, Hofmann G, Buccoliero AM, Paglierani M, Pollo B, Taddei GL, Gallina P, Di Lorenzo N, Franceschetti S, Wanke E, Arcangeli A. 2005. hERG1 channels are overexpressed in glioblastoma multiforme and modulate VEGF secretion in glioblastoma cell lines. *Br J Cancer* **93**:781-92. doi:10.1038/sj.bjc.6602775.

Moolenaar WH. 1986. Effects of growth factors on intracellular pH regulation. *Annu Rev Physiol* **48**:363-76. doi:10.1146/annurev.ph.48.030186.002051.

Moujaber O, Stochaj U. 2020. The Cytoskeleton as Regulator of Cell Signaling Pathways. *Trends Biochem Sci* **45**:96–107. doi:10.1016/j.tibs.2019.11.003.

Nelson M, Yang M, Dowle AA, Thomas JR, Brackenbury WJ. 2015. The sodium channel-blocking antiepileptic drug phenytoin inhibits breast tumour growth and metastasis. *Mol Cancer* **14**:13. doi:10.1186/S12943-014-0277-X.

Noegel A, Witke W, Schleicher M. 1987. Calcium-sensitive non-muscle alpha-actinin contains EF-hand structures and highly conserved regions. *FEBS Lett.* **221**(2):391-6. doi: 10.1016/0014-5793(87)80962-6. PMID: 3622778.

Onkal R, Djamgoz MBA. 2009. Molecular pharmacology of voltage-gated sodium channel expression in metastatic disease: clinical potential of neonatal Nav1.5 in breast cancer. *Eur J Pharmacol* **625**:206–219. doi:10.1016/j.ejphar.2009.08.040.

Onkal R, Mattis JH, Fraser SP, Diss JK, Shao D, Okuse K, Djamgoz MB. 2008. Alternative splicing of Nav1.5: An electrophysiological comparison of ‘neonatal’ and ‘adult’ isoforms and critical

involvement of a lysine residue. *J Cell Physiol* **216**:716–726. doi:10.1002/jcp.21451.

Otey CA, Vasquez GB, Burridge K, Erickson BW. 1993. Mapping of the alpha-actinin binding site within the beta 1 integrin cytoplasmic domain. *J Biol Chem* **268**:21193-7. PMID: 7691808.

Peretti M, Badaoui M, Girault A, Van Gulick L, Mabille MP, Tebbakha R, Sevestre H, Morjani H, Ouadid-Ahidouch H. 2019. Original association of ion transporters mediates the ECM-induced breast cancer cell survival: Kv10.1-Orai1-SPCA2 partnership. *Sci Rep* **9**:1175. doi:10.1038/s41598-018-37602-7.

Perez-Neut M, Rao VR, Gentile S. 2016. hERG1/Kv11.1 activation stimulates transcription of p21waf/cip in breast cancer cells via a calcineurin-dependent mechanism. *Oncotarget* **7**:58893–58902. doi:10.18632/oncotarget.3797.

Perou CM, Sørlie T, Eisen MB, van de Rijn M, Jeffrey SS, Rees CA, Pollack JR, Ross DT, Johnsen H, Akslen LA, Fluge O, Pergamenschikov A, Williams C, Zhu SX, Lønning PE, Børresen-Dale AL, Brown PO, Botstein D. 2000. Molecular portraits of human breast tumours. *Nat* **406**:747–752. doi: 10.1038/35021093.

Pillozzi S, Brizzi MF, Bernabei PA, Bartolozzi B, Caporale R, Basile V, Boddi V, Pegoraro L, Becchetti A, Arcangeli A. 2007. VEGFR-1 (FLT-1), beta1 integrin, and hERG K+ channel for a macromolecular signaling complex in acute myeloid leukemia: role in cell migration and clinical outcome. Blood. **110**(4):1238-50. doi: 10.1182/blood-2006-02-003772.

Pollard TD, Borisy GG. 2003. Cellular motility driven by assembly and disassembly of actin filaments. *Cell* **112**:453–465. doi:10.1016/s0092-8674(03)00120-x.

Ponce-Balbuena D, Guerrero-Serna G, Valdivia CR, Caballero R, Diez-Guerra FJ, Jiménez-Vázquez EN, Ramírez RJ, Monteiro da Rocha A, Herron TJ, Campbell KF, Willis BC, Alvarado FJ, Zarzoso M, Kaur K, Pérez-Hernández M, Matamoros M, Valdivia HH, Delpón E, Jalife J. 2018. Cardiac Kir2.1 and NaV1.5 Channels Traffic Together to the Sarcolemma to Control Excitability. *Circ Res* **122**:1501–1516. doi:10.1161/CIRCRESAHA.117.311872.

Potier-Cartereau M, Raoul W, Weber G, Mahéo K, Rapetti-Mauss R, Gueguinou M, Buscaglia P,

Goupille C, Le Goux N, Abdoul-Azize S, Lecomte T, Fromont G, Chantome A, Mignen O, Soriani O, Vandier C. 2022. Potassium and Calcium Channel Complexes as Novel Targets for Cancer Research. *Rev Physiol Biochem Pharmacol* **183**:157–176. doi:10.1007/112_2020_24.

Prevarskaya N, Skryma R, Shuba Y. 2018. Ion Channels in Cancer: Are Cancer Hallmarks Oncochannelopathies? *Physiol Rev* **98**:559–621. doi:10.1152/physrev.00044.2016.

Qiu Z, Dubin AE, Mathur J, Tu B, Reddy K, Miraglia LJ, Reinhardt J, Orth AP, Patapoutian A. 2014. SWELL1, a plasma membrane protein, is an essential component of volume-regulated anion channel. *Cell*. **157**(2):447-458. doi: 10.1016/j.cell.2014.03.024.

Rauhala HE, Teppo S, Niemelä S, Kallioniemi A. 2013. Silencing of the ARP2/3 complex disturbs pancreatic cancer cell migration. *Anticancer res* **33**:45-52. PMID:23267127.

Ridley AJ, Schwartz MA, Burridge K, Firtel RA, Ginsberg MH, Borisy G, Parsons JT, Horwitz AR. 2003. Cell migration: integrating signals from front to back. *Science.* **302**:1704–1709. doi: 10.1126/science.1092053.

Roger S, Besson P, Le Guennec JY. 2003. Involvement of a novel fast inward sodium current in the invasion capacity of a breast cancer cell line. *Biochim Biophys Acta - Biomembr* **1616**:107–111. doi:10.1016/j.bbamem.2003.07.001.

Santini L, Duranti C, Palandri C, Giammarino L, Musumeci M, Carlucci L, Capitani C, Colasurdo R, Recchia F, Cerbai E, Coppini R, Arcangeli A. 2023. Cardiac safety assessment of a novel recombinant bispecific antibody targeting the ether-à-go-go related gene 1 (hERG1)-β1 integrin macromolecular complex. *Front Pharmacol.* **14:**1237431. doi: 10.3389/fphar.2023.1237431.

Scarpellino G, Genova T, Avanzato D, Bernardini M, Bianco S, Petrillo S, Tolosano E, de Almeida Vieira JR, Bussolati B, Fiorio Pla A, Munaron L.2019. Purinergic Calcium Signals in -Derived Endothelium. *Cancers (Basel)* **11**:766. doi:10.3390/CANCERS11060766.

Sjöblom B, Salmazo A, Djinović-Carugo K. Alpha-actinin structure and regulation. 2008. *Cell Mol Life Sci.* Sep;65(17):2688-701. doi: 10.1007/s00018-008-8080-8.

Small JV, Stradal T, Vignal E, Rottner K. 2002. The lamellipodium: where motility begins. *Trends*

Cell Biol **12**:112–120. doi:10.1016/s0962-8924(01)02237-1.

Stoetzer C, Doll T, Stueber T, Herzog C, Echtermeyer F, Greulich F, Rudat C, Kispert A, Wegner F, Leffler A. 2016. Tetrodotoxin-sensitive α-subunits of voltage-gated sodium channels are relevant for inhibition of cardiac sodium currents by local anesthetics. *Naunyn Schmiedebergs Arch Pharmacol*. **389**:625-636. doi:10.1007/s00210-016-1231-9.

Sung H, Ferlay J, Siegel RL, Laversanne M, Soerjomataram I, Jemal A, Bray F. 2021. Global Cancer Statistics 2020: GLOBOCAN Estimates of Incidence and Mortality Worldwide for 36 Cancers in 185 Countries. *CA Cancer J Clin* **71**:209–249. doi:10.3322/caac.21660.

Swaney KF, Li R. 2016. Function and regulation of the Arp2/3 complex during cell migration in diverse environments. *Curr Opin Cell Biol* **42**:63-72. doi:10.1016/j.ceb.2016.04.005.

Takahashi K. 2001. The linkage between beta1 integrin and the actin cytoskeleton is differentially regulated by tyrosine and serine/threonine phosphorylation of beta1 integrin in normal and cancerous human breast cells. *BMC Cell Biol* **2**:23. doi:10.1186/1471-2121-2-23.

Tang S, Wang X, Shen Q, Yang X, Yu C, Cai C, Cai G, Meng X, Zou F. 2015. Mitochondrial Ca^{2+} uniporter is critical for store-operated Ca^{2+} entry-dependent breast cancer cell migration. *Biochem Biophys Res Commun* **458**:186–193. doi:10.1016/j.bbrc.2015.01.092.

Vargas P, Maiuri P, Bretou M, Sáez PJ, Pierobon P, Maurin M, Chabaud M, Lankar D, Obino D, Terriac E, Raab M, Thiam HR, Brocker T, Kitchen-Goosen SM, Alberts AS, Sunareni P, Xia S, Li R, Voituriez R, Piel M, Lennon-Duménil AM. 2016. Innate control of actin nucleation determines two distinct migration behaviours in dendritic cells. *Nat Cell Biol* **18**:43–53. doi: 0.1038/ncb3284.

Vogel V, Sheetz MP. 2006. Local force and geometry sensing regulate cell functions. *Nat. Rev. Mol. Cell Biol* **7**:265–275. doi:10.1038/nrm1890.

Wang W, Wyckoff JB, Frohlich VC, Oleynikov Y, Hüttelmaier S, Zavadil J, Cermak L, Bottinger EP, Singer RH, White JG, Segall JE, Condeelis JS. 2002. Single cell behavior in metastatic primary mammary s correlated with gene expression patterns revealed by molecular profiling. *Cancer res* **62**:6278-6288. PMID:12414658.

Wang W, Wyckoff JB, Goswami S, Wang Y, Sidani M, Segall JE, Condeelis JS. 2007. Coordinated regulation of pathways for enhanced cell motility and chemotaxis is conserved in rat and mouse mammary s. *Cancer res* **67**:3505-3511. doi:10.1158/0008-5472.CAN-06-3714.

Weaver AM., Karginov AV, Kinley AW, Weed SA, Li Y, Parsons JT, Cooper JA. 2001. Cortactin promotes and stabilizes Arp2/3-induced actin filament network formation. *Curr Biol* **11**:370-374. doi:10.1016/s0960-9822(01)00098-7.

White KA, Grillo-Hill BK, Barber DL. 2017. Cancer cell behaviors mediated by dysregulated pH dynamics at a glance. *J Cell Sci*. **130(**4):663-669. doi: 10.1242/jcs.195297. PMID: 28202602; PMCID: PMC5339414.

Wozniak MA, Modzelewska K, Kwong L, Keely PJ. 2004. Focal adhesion regulation of cell behavior. Biochim Biophys Acta. **1692**:103-19. doi:10.1016/j.bbamcr.2004.04.007.Yamaguchi H, Condeelis J. 2007. Regulation of the actin cytoskeleton in cancer cell migration and invasion. *Biochim Biophys Acta.* **1773**:642–652. doi:10.1016/j.bbamcr.2006.07.001.

Yang M, Kozminski DJ, Wold LA, Modak R, Calhoun JD, Isom LL, Brackenbury WJ. 2012. Therapeutic potential for phenytoin: targeting Na v 1.5 sodium channels to reduce migration and invasion in metastatic breast cancer. *Breast Cancer Res Treat* **134**:603–615. doi:10.1007/s10549-012-2102-9.

LEGENDS

Figure 1. The hERG1/ β1 integrin complex is expressed in breast cancer cell lines of different molecular subtype. A) Expression levels of the *KCNH2* transcripts, determined by Real Time PCR in different breast cancer cell lines (MCF-7, SKBR3, MDA-MB-231, MDA-MB-468), HEK-hERG1, and HEK-293 cells. HEK-hERG1 were used as positive control for *KCNH2*, HEK-293 as negative control. Cells were seeded onto Fibronectin (FN) for 2 hours. Data, reported as 2-DCt, are mean values ± s.e.m. (n=3). **B**) Expression levels of the hERG1 protein determined by Western Blot (WB) in breast cancer cell lines (MCF-7, SKBR3, MDA-MB-231, MDA-MB-468), HEK-hERG1 and HEK-293 cells. HEK-hERG1 were used as positive control for hERG1, HEK-293 as negative control for the two proteins. Cells were seeded onto FN for 2 hours. Representative WB (left panel) and densitometric analysis (right panel) are reported. Data are mean values ± s.e.m obtained in three independent experiments. a.u.= arbitrary units. **C)** Membrane expression levels of hERG1, determined by Immunofluorescence (IF) in breast cancer cell lines (MCF-7, SKBR3, MDA-MB-231, MDA-MB-468). Cells were seeded onto FN for 2 hours. Cells were stained for hERG1 (in green) with mAb-hERG1 primary antibody conjugated with AlexaFluor-488. Representative images (scale bar 100 µm) and quantification are reported. The quantification was performed considering only the membrane signal, highlighted by the white masks shown in the pictures. For each condition the fluorescence relative to 20 cells was analyzed. Full images are reported in Supplementary Figure 1A. Bar graph of normalized WB optical densities to the IF cytoplasmic values of hERG1. a.u.= arbitrary units. Pictures were taken on a confocal microscope (Nikon TE2000, Nikon; Minato, Tokyo, Japan). ImageJ software was used to analyse the images. **D)** Co-immunoprecipitation (co-IP) between hERG1 and β1 integrin in BCa cells (MCF-7, SKBR3, MDA-MB-231, MDA-MB-468) and HEK-293 (negative control) seeded onto FN for 2 hours. Immunoprecipitation was performed with a monoclonal antibody recognizing extracellular epitopes of the β1 integrin subunit (TS2/16) and a monoclonal antibody recognizing hERG1 (mAb-hERG1), left panels. Immunoprecipitation was performed with monoclonal antibody recognizing extracellular epitopes of hERG1, (right panel). Left

panels: representative experiment; right panels: densitometric analysis (n=3). Data are reported as a.u. (arbitrary unit). **E)** Co-immunoprecipitation of hERG1 with β1 integrins at T_{120}. Immunoprecipitation was performed with a monoclonal antibody recognizing extracellular epitopes of the β1 integrin subunit (TS2/16). Representative blots are in the top panels, the densitometric data are in the bottom panels. Data are mean values ± s.e.m. **F)** hERG1/β1 complex formation evaluated by staining with fluorescent scDb–hERG1–β1 in MDA-MB-231 and MDA-MB-468 cells seeded on FN. Representative IF images at T_{120} (left panel) (scale bars: 100 μm) and IF densitometric analysis (right panel) are reported. Full images are reported in Supplementary Figure 1B. Pictures were taken on a confocal microscope (Nikon TE2000, Nikon; Minato, Tokyo, Japan). ImageJ software was used to analyse the images. *P < 0.05 and **P < 0.01 and *** P < 0.001. IF = immunofluorescence. IP = immunoprecipitation.

Figure 2. The hERG1/β1 integrin complex is expressed in BCa cells, localizes in FAs and recruits α-actinin1 directly linked to β1 integrin A) Co-IP between β1 integrin and vinculin, paxillin, α-actinin, f-actin in BCa cells (MCF-7, SKBR3, MDA-MB-231, MDA-MB-468) and HEK-293 (negative control) seeded onto FN for 2 hours. Immunoprecipitation was performed with monoclonal antibody recognizing extracellular epitopes of the β1 integrin subunit (TS2/16). Data are reported as a. u. (arbitrary unit). **B)** Representative IF images (scale bar: 100 μm) of the co-localization of hERG1 (in green probed with mAb-hERG1 conjugated with AlexaFluor-488) and paxillin (in red probed with mAb-paxillin and secondary Ab conjugated with AlexaFluor-546) (top panel), and hERG1/β1 (in green probed with scDb-hERG1/β1 conjugated with AlexaFluor-488) and paxillin (in red probed with mAb-paxillin and secondary Ab conjugated with AlexaFluor-546) (bottom panel) in breast cancer cell lines (MCF-7, SKBR3, MDA-MB-231, MDA-MB-468) seeded onto FN for 2 hours. MOC reporting hERG1/paxillin and hERG1/β1/paxillin correlations is showed below each image. For each condition the fluorescence relative to 20 cells was analyzed. Full images are reported in Supplementary Figure 2A. Pictures were taken on a confocal microscope (Nikon

TE2000, Nikon; Minato, Tokyo, Japan). ImageJ software was used to analyse the images. **C)** Co-IP between hERG1, α-actinin1, and β1 integrin in BCa cells transiently silenced for hERG1. **D)** Co-IP between hERG1, α-actinin1, and β1 integrin in BCa cells transiently silenced for β1 integrin. Both in C) and D) BCa cells (MCF-7, SKBR3, MDA-MB-231, MDA-MB-468) were seeded onto FN for 2 hours. Immunoprecipitation was performed with monoclonal antibody TS2/16 (C) and monoclonal antibody for hERG1 (mAb-hERG1) (D). Data are mean values ± s.e.m obtained in three independent experiments. a.u.= arbitrary units. **E)** Model representation of the macromolecular complex comprising hERG1, β1 integrin and α-actinin1. Created with BioRender.com. MOC = Manders' Overlapping Coefficient. IP = immunoprecipitation. FN = fibronectin.

Figure 3. nNa$_V$1.5 is expressed in breast cancer cell lines of different molecular subtypes, in focal adhesions and is co-expressed with the hERG1/β1 integrin complex. A) Expression levels of the *nSCN5A* and *aSCN5A* transcripts determined by Real Time PCR in different breast cancer cell lines (MCF-7, SKBR3, MDA-MB-231, MDA-MB-468), EBNA-nNa$_V$1.5 and EBNA-aNa$_V$1.5. EBNA-nNa$_V$1.5 were used as positive control for *nSCN5A* while EBNA-aNa$_V$1.5 were used as negative control. Cells were seeded onto Fibronectin (FN) for 2 hours. Data, reported as 2-DCt, are mean values ± s.e.m. (n=3). **B)** Expression levels of nNa$_V$1.5, determined by Western Blot (WB) in breast cancer cell lines (MCF-7, SKBR3, MDA-MB-231, MDA-MB-468), EBNA-nNa$_V$1.5. EBNA-nNa$_V$1.5 as positive control for nNa$_V$1.5. Cells were seeded onto FN for 2 hours. Representative WB (left panel) and densitometric analysis (right panel) are reported. Data are mean values ± s.e.m obtained in three independent experiments. a.u.= arbitrary units. **C)** Membrane expression levels of nNa$_V$1.5, determined by Immunofluorescence (IF) in breast cancer cell lines (MCF-7, SKBR3, MDA-MB-231, MDA-MB-468). Cells were seeded onto FN for 2 hours. Cells were stained (in red) with mAb-nNa$_V$1.5 primary Ab conjugated with AlexaFluor-647. Representative images (scale bar 100 μm) and quantification are reported. The quantification was performed considering only the membrane signal, highlighted by the white masks shown in the pictures. For each condition the

fluorescence relative to 20 cells was analyzed. Full images are reported in Supplementary Figure 3A. Pictures were taken on a confocal microscope (Nikon TE2000, Nikon; Minato, Tokyo, Japan). ImageJ software was used to analyze the images. **D)** Co-immunoprecipitation **(**co-IP) between hERG1, $nNa_V1.5$ and β1 integrin in BCa cells (MCF-7, SKBR3, MDA-MB-231, MDA-MB-468) and HEK-293 (negative control) seeded onto FN for 2 hours. Immunoprecipitation was performed with monoclonal antibody recognizing extracellular epitopes of the β1 integrin subunit (TS2/16), and a monoclonal antibody recognizing hERG1 (mAb-hERG1), left panels. **Left panel:** representative experiment; **right panel:** densitometric analysis (n=3). Data are reported as a. u. (arbitrary unit). *P < 0.05 and **P < 0.01. IP = immunoprecipitation.

Figure 4. hERG1, β1, $nNa_V1.5$ form a tri-molecular complex which is localized in focal adhesions. A) Representative IF images (scale bar: 100 μm) of the co-localization of hERG1, β1 integrin hERG1 (in green probed with scDb-hERG1-β1 conjugated with alexa-488) and $nNa_V1.5$ (in red probed with mAb-$nNa_V1.5$ conjugated with AlexaFluor-647) in breast cancer cell lines (MCF-7, SKBR3, MDA-MB-231, MDA-MB-468) seeded onto FN for 2 hours. Mander's Overlapping Coefficient (MOC) reporting the proteins correlation is showed below each image. For each condition the fluorescence relative to 20 cells was analyzed. Full images are reported in Supplementary Figure 4A. Pictures were taken on a confocal microscope (Nikon TE2000, Nikon; Minato, Tokyo, Japan). ImageJ software was used to analyse the images. **B)** Co-IP between hERG1, $nNa_V1.5$, and β1 integrin in BCa transiently transiently β1 integrin and **C)** hERG1 silenced cells (MCF-7, SKBR3, MDA-MB-231, MDA-MB-468) seeded onto FN for 2 hours. Immunoprecipitation was performed with monoclonal antibody recognizing hERG1 (mAb-hERG1) and monoclonal antibody TS2/16. Data are mean values ± s.e.m obtained in three independent experiments. a.u.= arbitrary units. **D)** Representative IF images (scale bar: 100 μm) of the co-localization of $nNa_V1.5$ (in green probed with mAb-$nNa_V1.5$ conjugated with AlexaFluor-488) and paxillin (in red probed with mAb-paxillin and secondary Ab conjugated with AlexaFluor-546) (bottom panel) in breast cancer cell lines (MCF-7,

SKBR3, MDA-MB-231, MDA-MB-468) seeded onto FN for 2 hours. MOC reporting $nNa_V1.5$/paxillin correlations is showed below each image. For each condition the fluorescence relative to 20 cells was analyzed. Full images are reported in Supplementary Figure 4B. Pictures were taken on a confocal microscope (Nikon TE2000, Nikon; Minato, Tokyo, Japan). ImageJ software was used to analyse the images. **E)** Model representation of the macromolecular complex comprising hERG1, β1 integrin, α-actinin and $nNa_V1.5$. Created with BioRender.com. IP = immunoprecipitation. MOC = Manders' Overlapping Coefficient.

Figure 5. The expression of hERG1 and $nNa_V1.5$ is mutually regulated in BCa cells. WB revealing hERG1, $nNa_V1.5$ and β1 integrin in BCa transiently hERG1 (**A)** and $nNa_V1.5$ (**B**) silenced cells (MCF-7, SKBR3, MDA-MB-231, MDA-MB-468) seeded onto FN for 2 hours. Left panel: representative experiment; right panel: densitometric analysis. Data are mean values ± s.e.m obtained in three independent experiments. a.u.= arbitrary units. **C)** Expression levels of the two transcripts, *KCNH2* and *nSCN5A*, determined by Real Time PCR in MDA-MB-231 and MDA-MB-231-T cell lines. Data, reported as 2-DCt, are mean values ± s.e.m. (n=3). **D)** Expression levels of the two proteins, hERG1 and $nNa_V1.5$, determined by WB in MDA-MB-231 and MDA-MB-231-T cell lines. Representative WB (top panel) and densitometric analysis (bottom panel) are reported. Data are mean values ± s.e.m obtained in three independent experiments. **E)** On the left, patch clamp hERG1 inward current trace and activation curve of a representative MDA-MB-231 and MDA-MB-231-T cell. Patch clamp hERG1 inward current trace recorded in MDA-MB-231 cells shown below it. On the right Na^+ traces recorded in MDA-MB-231 and MDA-MB-231-T cells. Data are mean values ± s.e.m obtained in three independent experiments. For all experiments of lateral motility and invasiveness, a background level of invasion was calculated, seeding cells without chemotactic gradient, and a basal level of invasion was then subtracted from the experiment measurements. $^{**}P < 0.01$ and $^{***}P < 0.001$. IP = immunoprecipitation. WB = Western Blot.

Figure 6. hERG1 and nNav1.5 form a macromolecular complex with β1 integrins which is inhibited by either hERG1 or Nav blockers. A) WB of all TNBCa cell lines treated with E4031 (40 μM) and **B)** with TTX (20μM) with the respective densitometric analysis **C)** in panel below. All the quantification were normalized against control (not shown). **D)** co-IP between hERG1, nNav1.5 and β1 integrin in BCa cells (MCF-7, SKBR3, MDA-MB-231, MDA-MB-468) seeded onto FN for 2 hours and treated with E4031 (40μM) and TTX (20μM). Immunoprecipitation was performed with monoclonal antibody TS2/16. **E)** Densitometric analysis. Data are mean values ± s.e.m obtained in three independent experiments. a.u.= arbitrary units. **P < 0.01 and ***P < 0.001. IP = immunoprecipitation. WB = Western Blot.

Figure 7. hERG1 and nNav1.5 modulates the organization of f-actin. A) Staining with anti-Arp2/3 (green) antibody with secondary Ab AlexaFluor-488 and CellMask™ Deep Red Actin Tracking Stain (red) of MDA-MB-231 and MDA-MB-468 cells seeded on FN for 2 hours and treated with E4031: 40μM, scDb-hERG1/β1: 20μg/ml and TTX: 20μM. Corresponding Arp2/3 graphs on the right panel. **B)** Phalloidin staining (Ab conjugated with Rhodamine) of MDA-MB-231 and MDA-MB-468 cells seeded on FN for 2 hours and treated with E4031: 40μM, scDb-hERG1/β1: 20μg/ml and TTX: 20μM. Corresponding graphs of actin stress fibers length, filopodia length and cortical actin density. **C)** Staining with anti-cortactin antibody of MDA-MB-231 and MDA-MB-468 cells seeded on FN for 2 hours and treated with E4031: 40μM, scDb-hERG1/β1: 20μg/ml and TTX: 20μM. Corresponding graphs of the percentage of cells that show invadopodia. At least 20 cells per condition were analyzed and all p-values were determined by a Mann–Whitney test for non-parametric values, or for data deviating from normality by a Kolmogorov–Smirnov test. Scale bars: 10 μm. Full images for all panels are reported in Supplementary Figure 6A, B & C. Pictures were taken on a confocal microscope (Nikon TE2000, Nikon; Minato, Tokyo, Japan). ImageJ software was used to analyse the images. In the graphs, boxes include central 50% of data points, the horizontal lines denote minimum

value, median and maximum value. Data are mean values ± s.e.m. (*n*=3). *P < 0.05, **P < 0.01 and **P < 0.001. IF = immunofluorescence. FN = Fibronectin.

Figure 8. The signaling pathways downstream to the hERG1/β1 integrin/nNaV1.5 complex

A) The intracellular Ca^{2+} has been also measured under different conditions. MCF-7 and MDA-MB-468 have been seeded on different type of coating method: FN and BSA for 2h and then intracellular Ca^{2+} was measured as reported in Materials and Methods. Image acquisition (3s frequency) was performed using Metafluor Imaging System (Molecular Devices; Sunnyvale, CA, USA). **B)** pAKT levels were determined by Western Blot (WB) in MCF-7 and MDA-MB-468 while cells were treated with specific blockers E4301 (40µM), TTX (20µM) and scDb-hERG1-β1 (20µg/ml) in different coating conditions (BSA and FN for 2h). Representative WB (top panel) and densitometric analysis (bottom panel) are reported. Data are mean values ± s.e.m obtained in three independent experiments. a.u.= arbitrary units. **C)** pH_i values of MCF-7, SKBR3, MDA-MB-231 and MDA-MB-468 cell lines seeded for 2h onto FN and treated with E4031 (40µM), TTX (20µM), cariporide (5µM), scDb-hERG1-β1 (20µg/ml) and Ouabain (300nM). All pH values were calculated using 490/440nm fluorescence ratio and applying standard curve and linear equations. Data are mean values ± s.e.m obtained in three independent experiments. *P < 0.05, **P < 0.01 and ***P < 0.001. R = ratio.

Figure 9. The hERG1/β1/nNaV1.5 complex comprises the Na^+/H^+ exchanger NHE1. Effects of the NHE1 inhibitor cariporide on f-actin organization in TNBCa cells. A) co-IP between hERG1, nNaV1.5, NHE1 and β1 integrin in BCa transiently hERG1 and **(B)** β1 silenced cells (MCF-7, SKBR3, MDA-MB-231, MDA-MB-468) seeded onto FN for 2 hours. Immunoprecipitation was performed with monoclonal antibody TS2/16 (A) and monoclonal antibody recognizing hERG1 (mAb-hERG1) (B). In the graphs, boxes include central 50% of data points, the horizontal lines denote minimum value, median and maximum value. Data are mean values ± s.e.m. (*n*=3). **C)** Phalloidin (conjugated with rhodamine) staining of MDA-MB-231 and MDA-MB-468 cells seeded on FN for 2 hours and

treated with Cariporide (5μM). Representative images are on the top part of the panel, the corresponding graph of actin stress fibres length, filopodia length and density are below. At least 20 cells per condition were analyzed and all p-values were determined by a Mann–Whitney test, or for data deviating from normality by a Kolmogorov–Smirnov test. Scale bars: 10 μm. Full images are reported in Supplementary Figure 8C. Pictures were taken on a confocal microscope (Nikon TE2000, Nikon; Minato, Tokyo, Japan). ImageJ software was used to analyse the images. **D)** Model representation of the macromolecular complex comprising hERG1, β1 integrin, α-actinin, $nNa_V1.5$ and NHE1. Created with BioRender.com. IP = immunoprecipitation. *P < 0.05, **P < 0.01.

Figure 10. hERG1 and $nNa_V1.5$ control cell motility and invasiveness in BCa cell lines. A) Cell proliferation determined by MTT test in MCF-7, SKBR3, MDA-MB-231 and MDA-MB-468 and cell lines. Cells were treated with E4031 (40μM), tetrodotoxin (TTX) (20μM) and scDb-hERG1-β1 (20μg/ml) for 24 hours and absorbance at 570n was measured. **B)** Motility Index (MoI) determined by lateral motility experiments in MCF-7, SKBR3, MDA-MB-231 and MDA-MB-468 cell lines. Cells were treated with E4031 (40μM), tetrodotoxin (TTX) (20μM), scDb-hERG1-β1 (20μg/ml), cariporide (5μM) and a combination of the latters. Data are mean values ± s.e.m obtained in three independent experiments. **C)** Invasiveness obtained with matrigel invasion assay in MCF-7, SKBR3, MDA-MB-231 and MDA-MB-468 cell lines. Cells were treated with E4031 (40μM), tetrodotoxin (TTX) (20μM), scDb-hERG1-β1 (20μg/ml), cariporide (5μM) and a combination of the latters for 24 hours and cells per mm^2 were counted. Data are mean values ± s.e.m obtained in three independent experiments. The number of cells counted in each field of view was converted to "cells per mm^2" by multiplying the number of counted cells by a factor of 4.07. For all experiments of lateral motility and invasiveness, a background level of invasion was calculated, seeding cells without chemotactic gradient, and a basal level of invasion was then subtracted from the experiment measurements. *P < 0.05, **P < 0.01 and **P < 0.001.

Figure 11. The integrin-centered macromolecular signaling complex in BCa cells.

In cells adhering to FN a macromolecular complex is formed which comprises hERG1, the β1 integrin subunit and the neonatal form of $Na_V1.5$. The β1 integrin associates with α-actinin which directly modulates f-actin organization. hERG1 also associates with the NHE-1 exchanger whose activation increases the intracellular pH and impacts on f-actin organization. The f-actin remodeling leads to the formation of invadopodia. Created with BioRender.com.

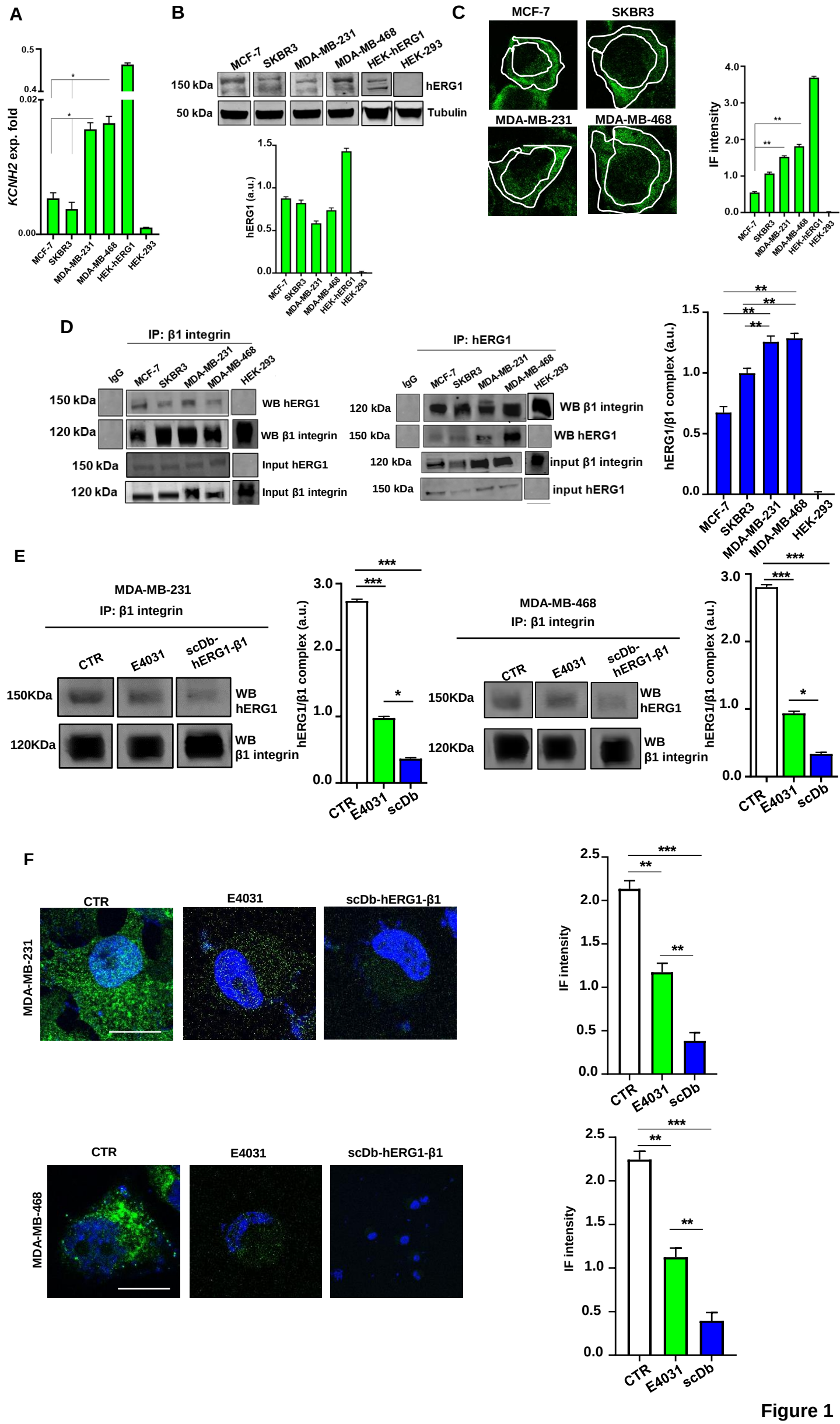
A
KCNH2 exp. fold
MCF-7
SKBR3
MDA-MB-231
MDA-MB-468
HEK-hERG1
HEK-293
B
150 kDa
50 kDa
hERG1
Tubulin
hERG1 (a.u.)
C
IF intensity
D
IP: β1 integrin
IgG
WB hERG1
WB β1 integrin
Input hERG1
Input β1 integrin
IP: hERG1
input β1 integrin
input hERG1
hERG1/β1 complex (a.u.)
E
MDA-MB-231
MDA-MB-468
CTR
E4031
scDb-hERG1-β1
150KDa
120KDa
WB hERG1
WB β1 integrin
scDb
F
IF intensity

Figure 1

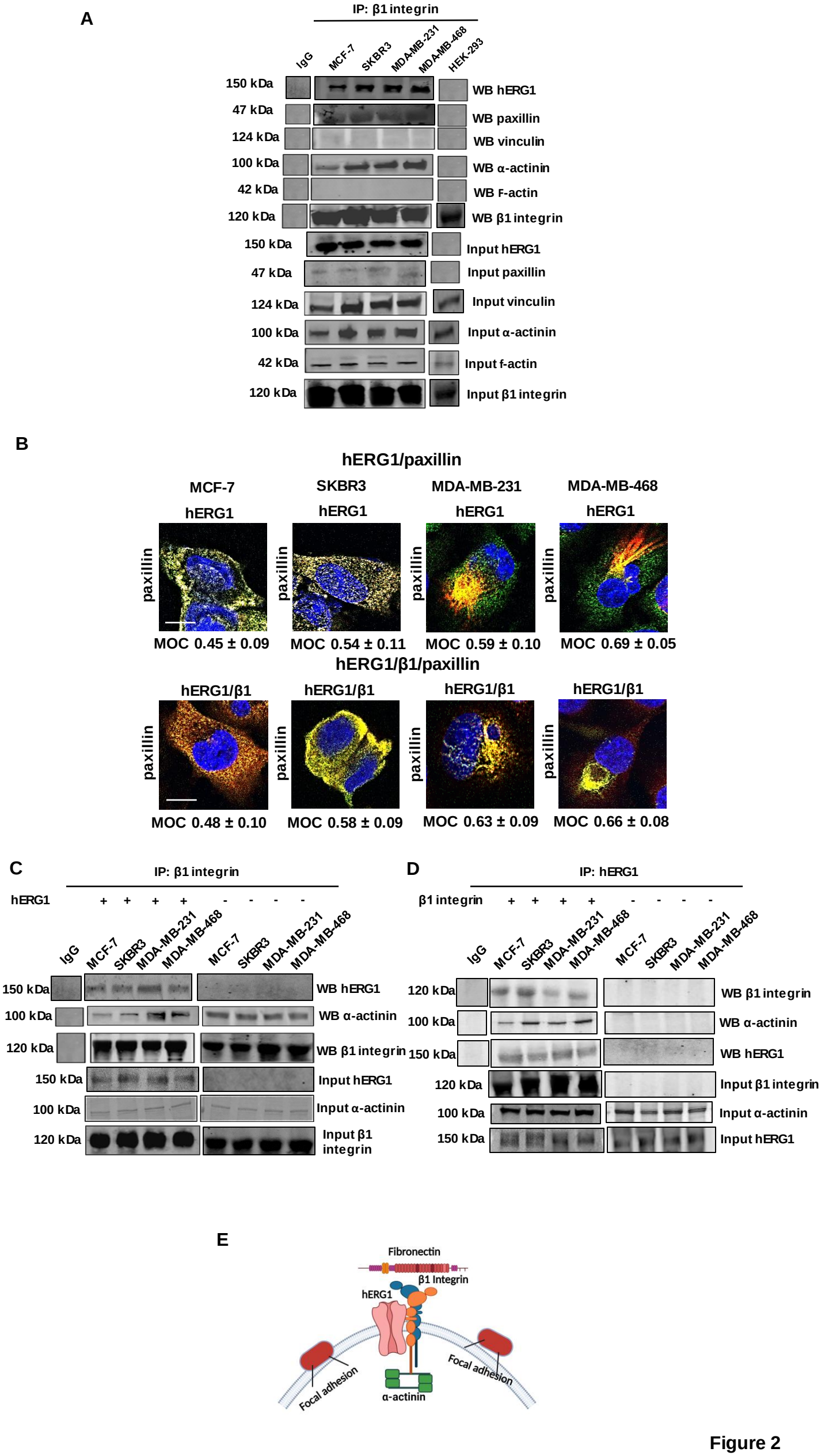
A
IP: β1 integrin
IgG
MCF-7
SKBR3
MDA-MB-231
MDA-MB-468
HEK-293
150 kDa
WB hERG1
47 kDa
WB paxillin
124 kDa
WB vinculin
100 kDa
WB α-actinin
42 kDa
WB F-actin
120 kDa
WB β1 integrin
150 kDa
Input hERG1
47 kDa
Input paxillin
124 kDa
Input vinculin
100 kDa
Input α-actinin
42 kDa
Input f-actin
120 kDa
Input β1 integrin
B
hERG1/paxillin
MCF-7
SKBR3
MDA-MB-231
MDA-MB-468
hERG1
paxillin
MOC 0.45 ± 0.09
MOC 0.54 ± 0.11
MOC 0.59 ± 0.10
MOC 0.69 ± 0.05
hERG1/β1/paxillin
hERG1/β1
MOC 0.48 ± 0.10
MOC 0.58 ± 0.09
MOC 0.63 ± 0.09
MOC 0.66 ± 0.08
C
IP: β1 integrin
hERG1
+ + + + - - - -
IgG
MCF-7
SKBR3
MDA-MB-231
MDA-MB-468
150 kDa
WB hERG1
100 kDa
WB α-actinin
120 kDa
WB β1 integrin
150 kDa
Input hERG1
100 kDa
Input α-actinin
120 kDa
Input β1 integrin
D
IP: hERG1
β1 integrin
+ + + + - - - -
IgG
MCF-7
SKBR3
MDA-MB-231
MDA-MB-468
120 kDa
WB β1 integrin
100 kDa
WB α-actinin
150 kDa
WB hERG1
120 kDa
Input β1 integrin
100 kDa
Input α-actinin
150 kDa
Input hERG1
E
Fibronectin
β1 Integrin
hERG1
Focal adhesion
α-actinin
Focal adhesion

Figure 2

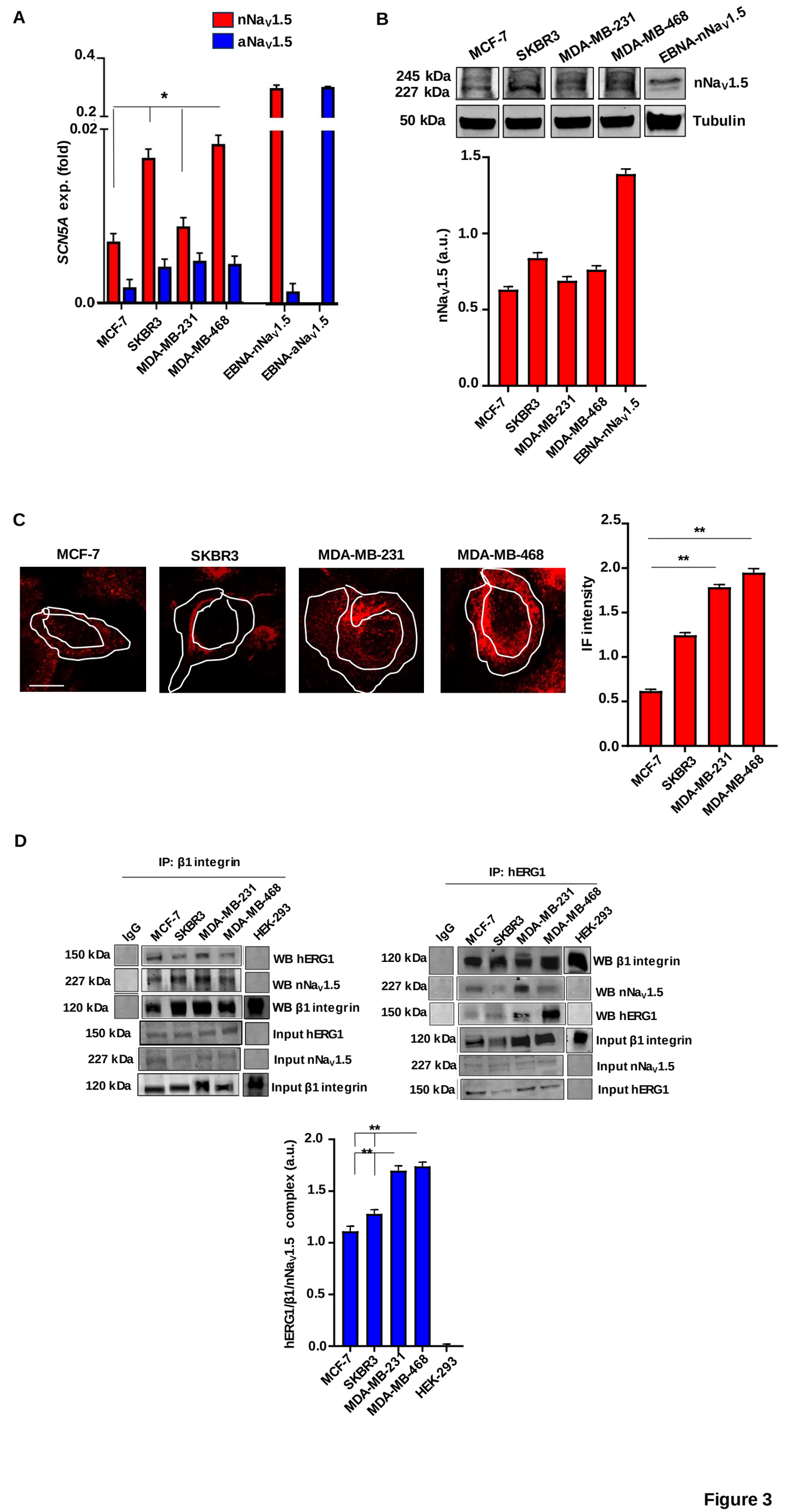
A
nNaV1.5
aNaV1.5
SCN5A exp. (fold)
0.4
0.2
0.02
0.0
*
MCF-7
SKBR3
MDA-MB-231
MDA-MB-468
EBNA-nNaV1.5
EBNA-aNaV1.5
B
MCF-7
SKBR3
MDA-MB-231
MDA-MB-468
EBNA-nNaV1.5
245 kDa
227 kDa
nNaV1.5
50 kDa
Tubulin
nNaV1.5 (a.u.)
1.5
1.0
0.5
0.0
C
MCF-7
SKBR3
MDA-MB-231
MDA-MB-468
IF intensity
2.5
2.0
1.5
1.0
0.5
0.0
**
**
D
IP: β1 integrin
IgG
HEK-293
150 kDa
227 kDa
120 kDa
WB hERG1
WB nNaV1.5
WB β1 integrin
Input hERG1
Input nNaV1.5
Input β1 integrin
IP: hERG1
hERG1/β1/nNaV1.5 complex (a.u.)

Figure 3

A

hERG1/ β1/nNa$_V$1.5

MCF-7 hERG1/β1 — nNa$_V$1.5

MOC 0.42 ± 0.05

SKBR3 hERG1/β1 — nNa$_V$1.5

MOC 0.50 ± 0.10

MDA-MB-231 hERG1/β1 — nNa$_V$1.5

MOC 0.51 ± 0.08

MDA-MB-468 hERG1/β1 — nNa$_V$1.5

MOC 0.76 ± 0.04

B

IP: hERG1

β1 integrin + + + + - - - -

IgG | MCF-7 | SKBR3 | MDA-MB-231 | MDA-MB-468 | MCF-7 | SKBR3 | MDA-MB-231 | MDA-MB-468

120 kDa — WB β1 integrin

227 kDa — WB nNa$_V$1.5

150 kDa — WB hERG1

120 kDa — Input β1 integrin

227 kDa — Input nNa$_V$1.5

150 kDa — Input hERG1

C

IP: β1 integrin

hERG1 + + + + - - - -

IgG | MCF-7 | SKBR3 | MDA-MB-231 | MDA-MB-468 | MCF-7 | SKBR3 | MDA-MB-231 | MDA-MB-468

150 kDa — WB hERG1

227 kDa — WB nNa$_V$1.5

120 kDa — WB β1 integrin

150 kDa — Input hERG1

227 kDa — Input nNa$_V$1.5

120 kDa — Input β1 integrin

D

nNa$_V$1.5/paxillin

MCF-7 nNa$_V$1.5 — paxillin

MOC 0.39 ± 0.11

SKBR3 nNa$_V$1.5 — paxillin

MOC 0.40 ± 0.07

MDA-MB-231 nNa$_V$1.5 — paxillin

MOC 0.50 ± 0.08

MDA-MB-468 nNa$_V$1.5 — paxillin

MOC 0.62 ± 0.06

E

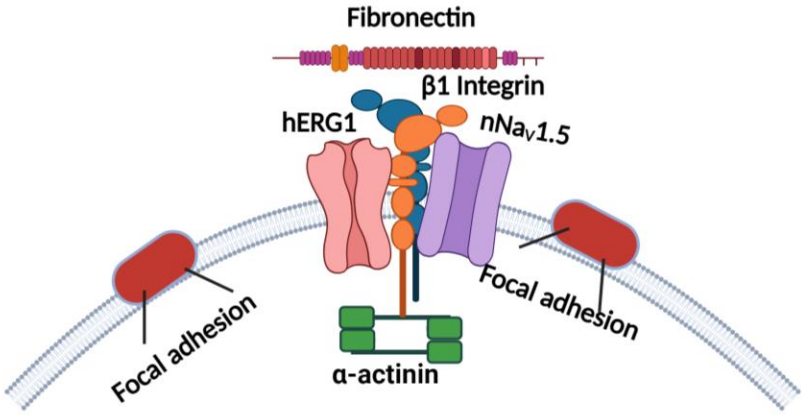

Figure 4

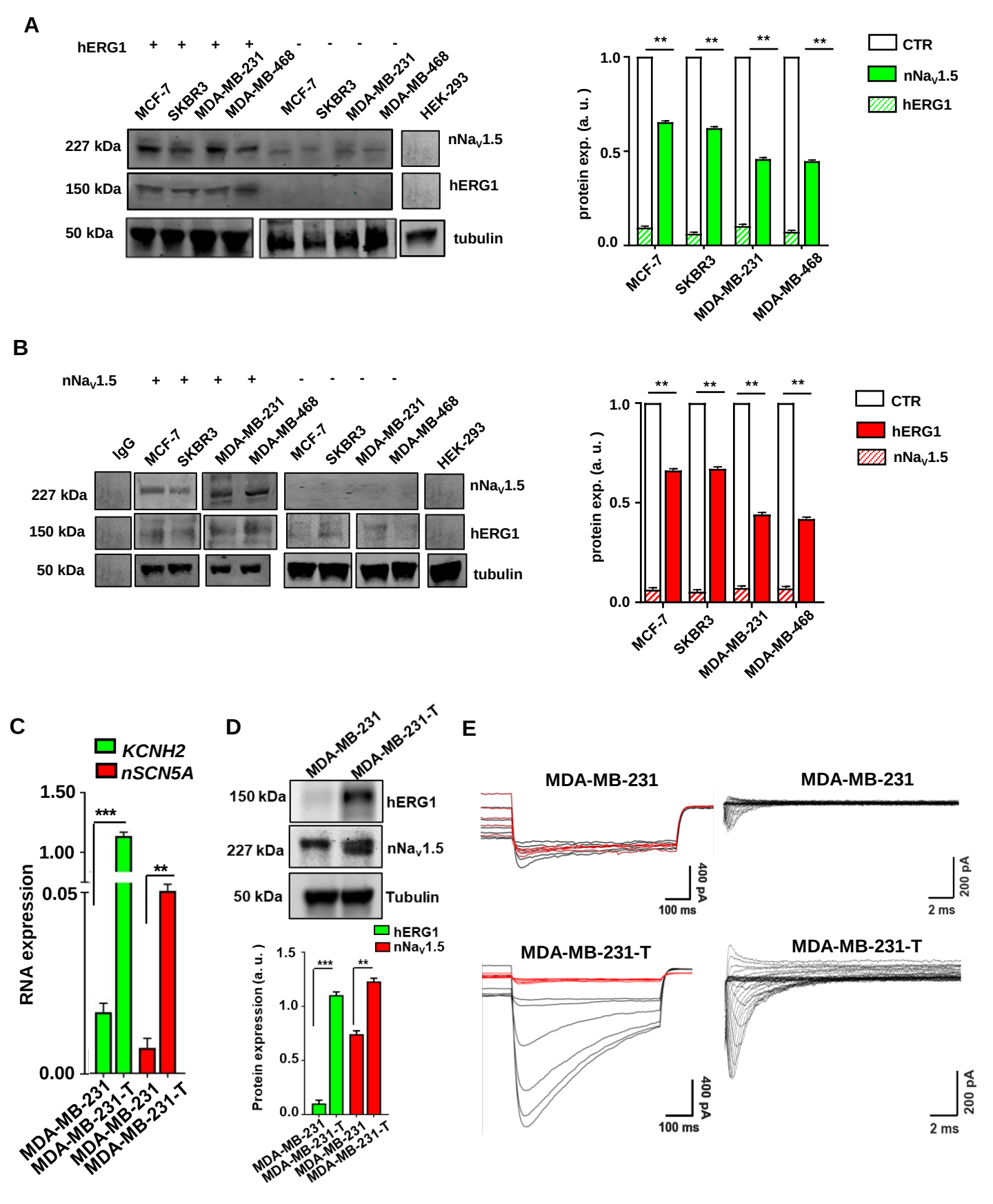
A
hERG1
MCF-7
SKBR3
MDA-MB-231
MDA-MB-468
HEK-293
227 kDa
150 kDa
50 kDa
nNaV1.5
hERG1
tubulin
protein exp. (a. u.)
CTR
B
IgG
C
KCNH2
nSCN5A
RNA expression
MDA-MB-231-T
D
Protein expression (a. u.)
E
400 pA
100 ms
200 pA
2 ms

Figure 5

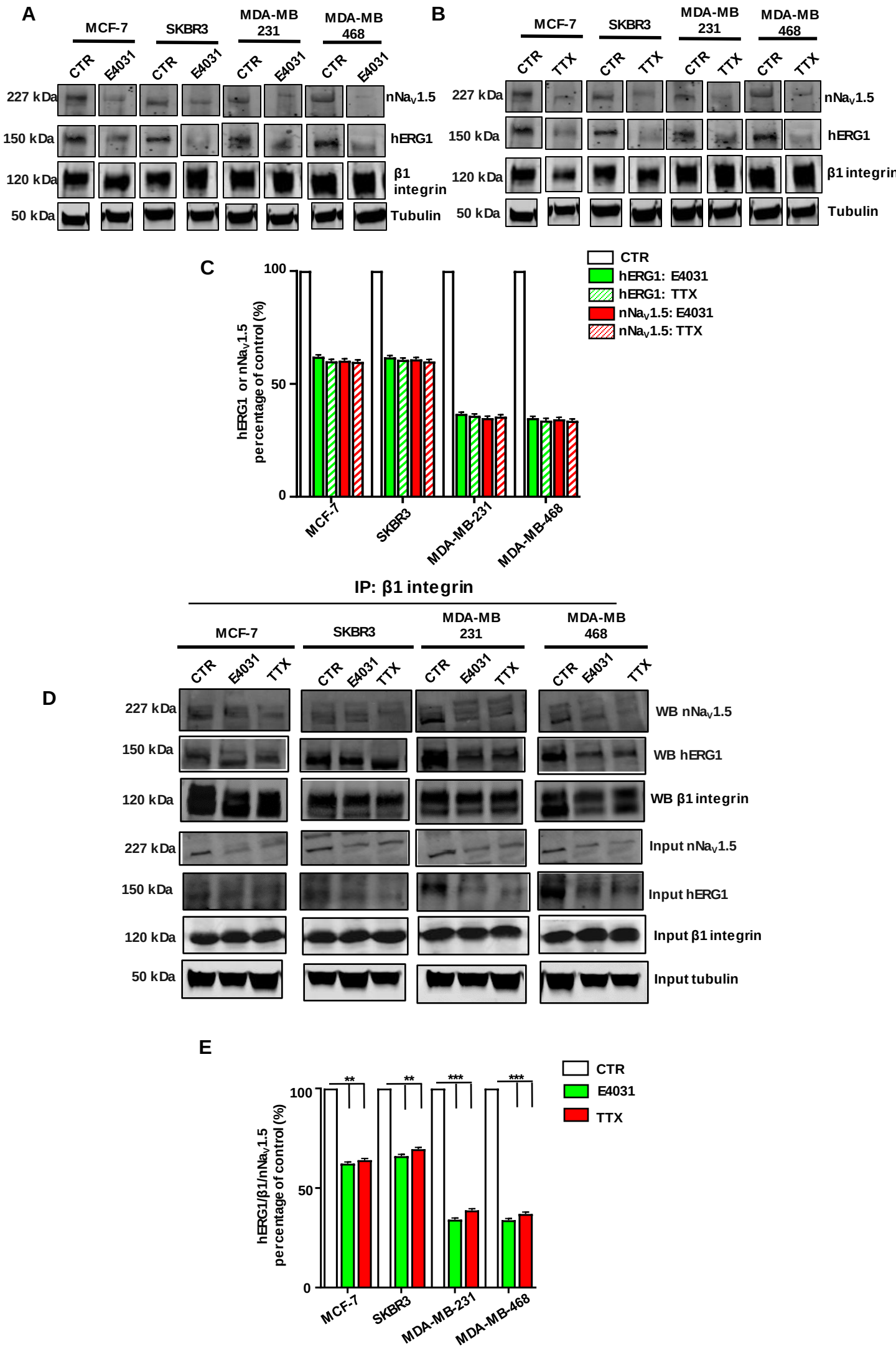
A
MCF-7
SKBR3
MDA-MB 231
MDA-MB 468
CTR
E4031
227 kDa
150 kDa
120 kDa
50 kDa
nNaV1.5
hERG1
β1 integrin
Tubulin
B
TTX
C
hERG1 or nNaV1.5 percentage of control (%)
100
50
0
CTR
hERG1: E4031
hERG1: TTX
nNaV1.5: E4031
nNaV1.5: TTX
MCF-7
SKBR3
MDA-MB-231
MDA-MB-468
IP: β1 integrin
D
WB nNaV1.5
WB hERG1
WB β1 integrin
Input nNaV1.5
Input hERG1
Input β1 integrin
Input tubulin
E
hERG1/β1/nNaV1.5 percentage of control (%)
**
***

Figure 6

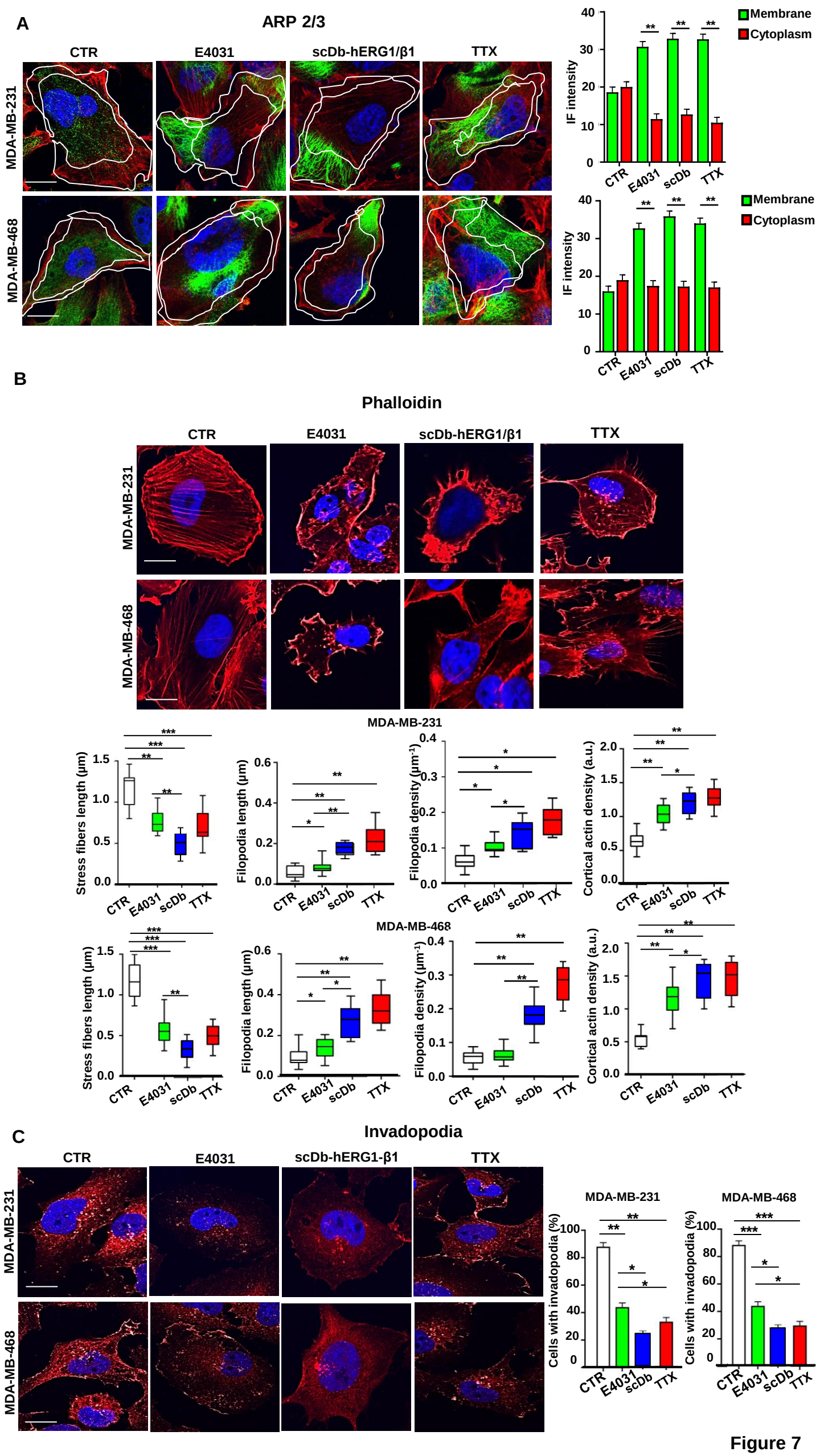
A
ARP 2/3
CTR
E4031
scDb-hERG1/β1
TTX
MDA-MB-231
MDA-MB-468
Membrane
Cytoplasm
IF intensity
CTR
E4031
scDb
TTX
B
Phalloidin
CTR
E4031
scDb-hERG1/β1
TTX
MDA-MB-231
MDA-MB-468
Stress fibers length (µm)
Filopodia length (µm)
Filopodia density (µm⁻¹)
Cortical actin density (a.u.)
CTR
E4031
scDb
TTX
C
Invadopodia
CTR
E4031
scDb-hERG1-β1
TTX
MDA-MB-231
MDA-MB-468
Cells with invadopodia (%)
CTR
E4031
scDb
TTX

Figure 7

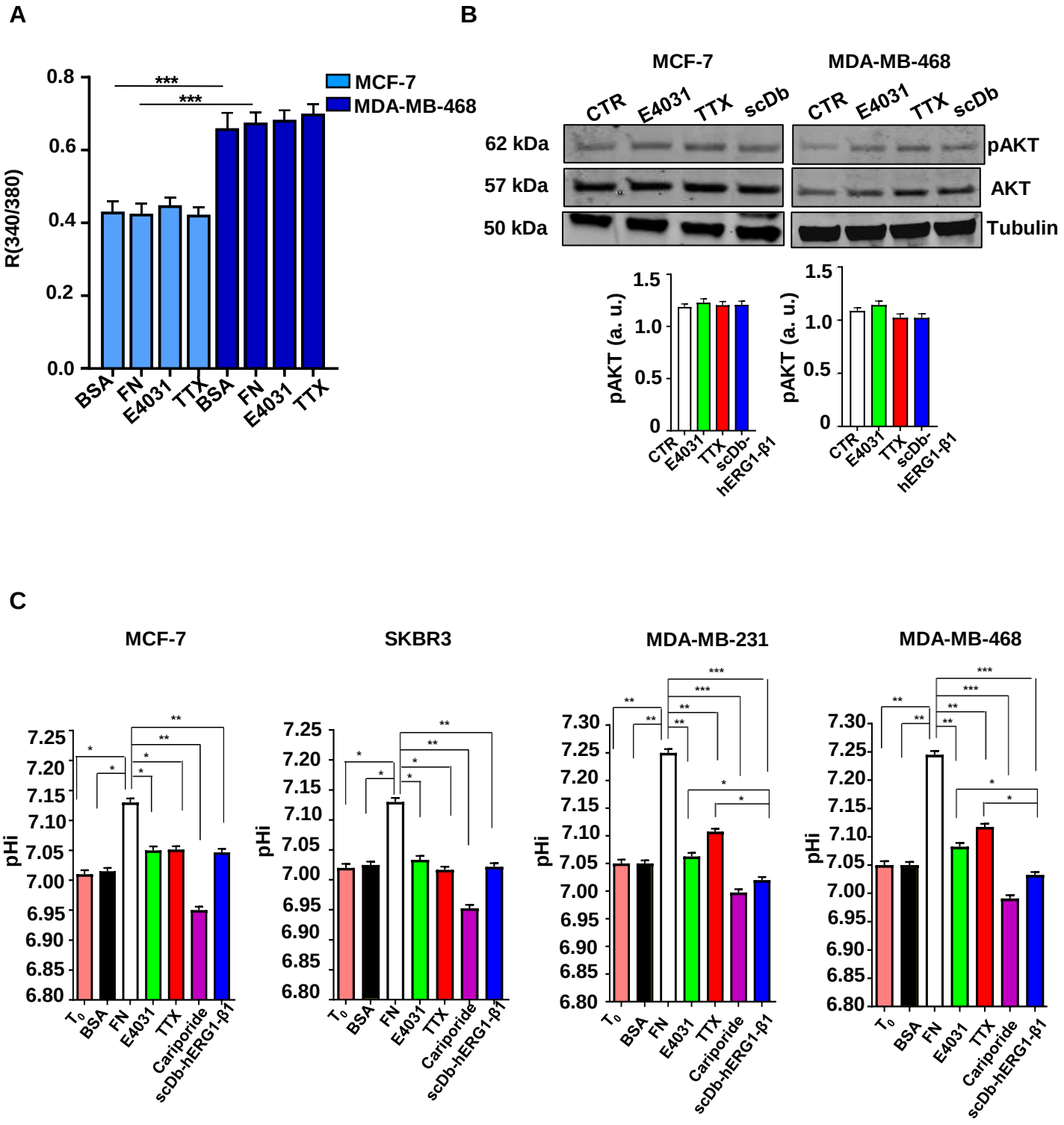
A
R(340/380)
0.8
0.6
0.4
0.2
0.0
***
***
MCF-7
MDA-MB-468
BSA
FN
E4031
TTX
BSA
FN
E4031
TTX
B
MCF-7
MDA-MB-468
CTR
E4031
TTX
scDb
CTR
E4031
TTX
scDb
62 kDa
57 kDa
50 kDa
pAKT
AKT
Tubulin
pAKT (a. u.)
1.5
1.0
0.5
0
CTR
E4031
TTX
scDb-hERG1-β1
C
MCF-7
SKBR3
MDA-MB-231
MDA-MB-468
pHi
7.30
7.25
7.20
7.15
7.10
7.05
7.00
6.95
6.90
6.85
6.80
T0
BSA
FN
E4031
TTX
Cariporide
scDb-hERG1-β1

Figure 8

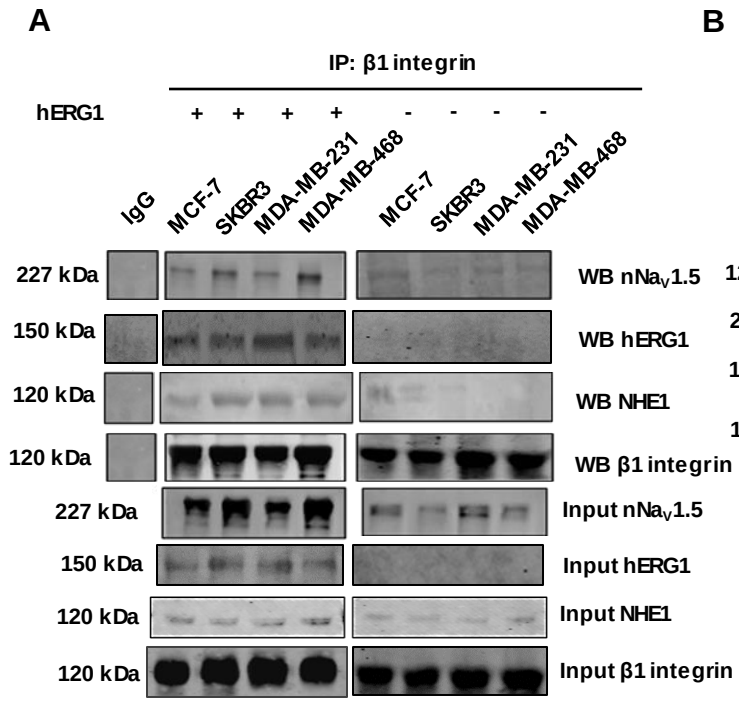
A
IP: β1 integrin
hERG1
+ + + + - - - -
IgG
MCF-7
SKBR3
MDA-MB-231
MDA-MB-468
MCF-7
SKBR3
MDA-MB-231
MDA-MB-468
227 kDa
150 kDa
120 kDa
120 kDa
227 kDa
150 kDa
120 kDa
120 kDa
WB nNa$_V$1.5
WB hERG1
WB NHE1
WB β1 integrin
Input nNa$_V$1.5
Input hERG1
Input NHE1
Input β1 integrin

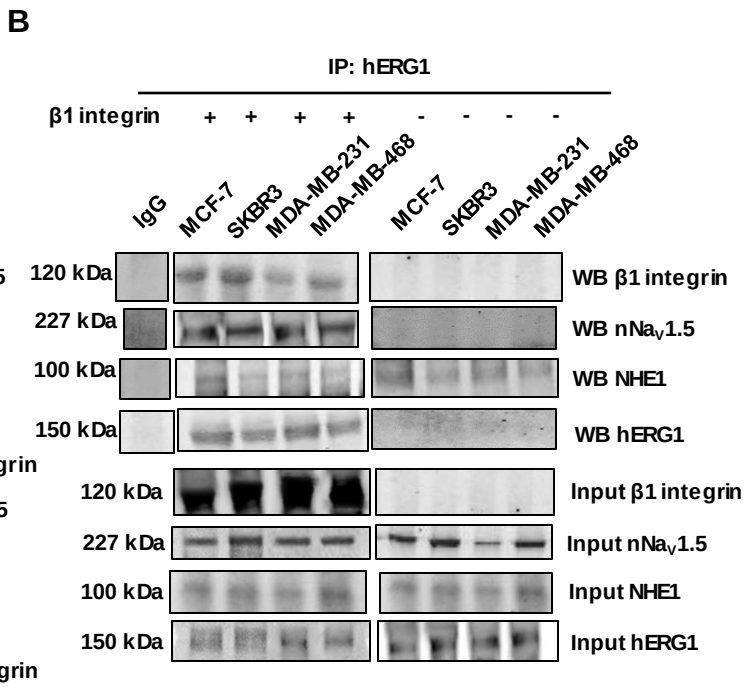
B
IP: hERG1
β1 integrin
+ + + + - - - -
IgG
MCF-7
SKBR3
MDA-MB-231
MDA-MB-468
MCF-7
SKBR3
MDA-MB-231
MDA-MB-468
120 kDa
227 kDa
100 kDa
150 kDa
120 kDa
227 kDa
100 kDa
150 kDa
WB β1 integrin
WB nNa$_V$1.5
WB NHE1
WB hERG1
Input β1 integrin
Input nNa$_V$1.5
Input NHE1
Input hERG1

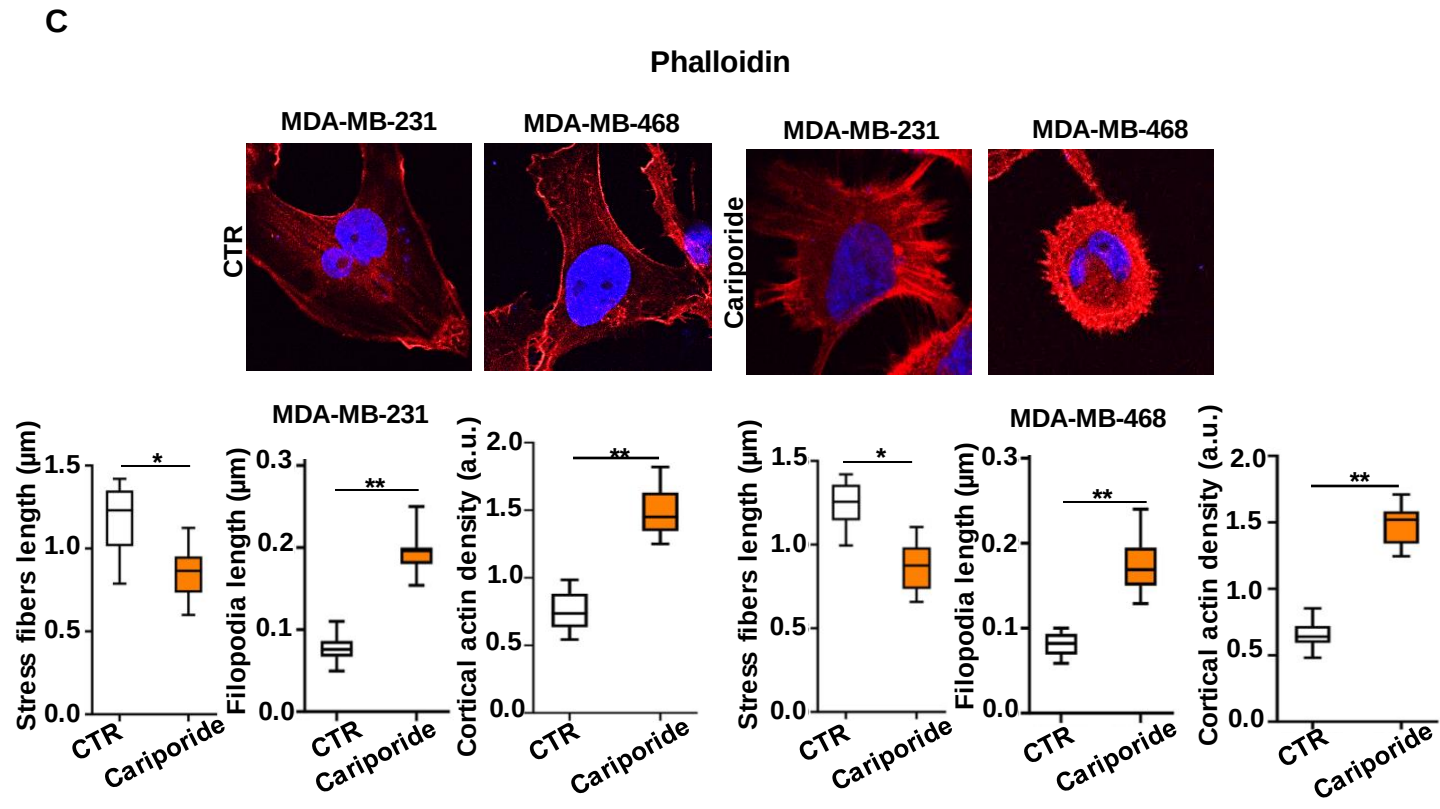
C
Phalloidin
MDA-MB-231
MDA-MB-468
MDA-MB-231
MDA-MB-468
CTR
Cariporide
MDA-MB-231
Stress fibers length (µm)
Filopodia length (µm)
Cortical actin density (a.u.)
MDA-MB-468
Stress fibers length (µm)
Filopodia length (µm)
Cortical actin density (a.u.)
CTR
Cariporide
*
**

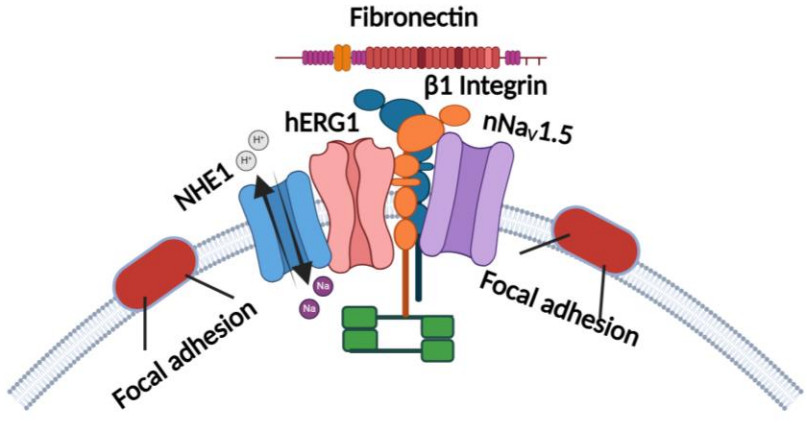
F
Fibronectin
β1 Integrin
hERG1
nNa$_V$1.5
NHE1
H+
Na
Focal adhesion
Focal adhesion

Figure 9

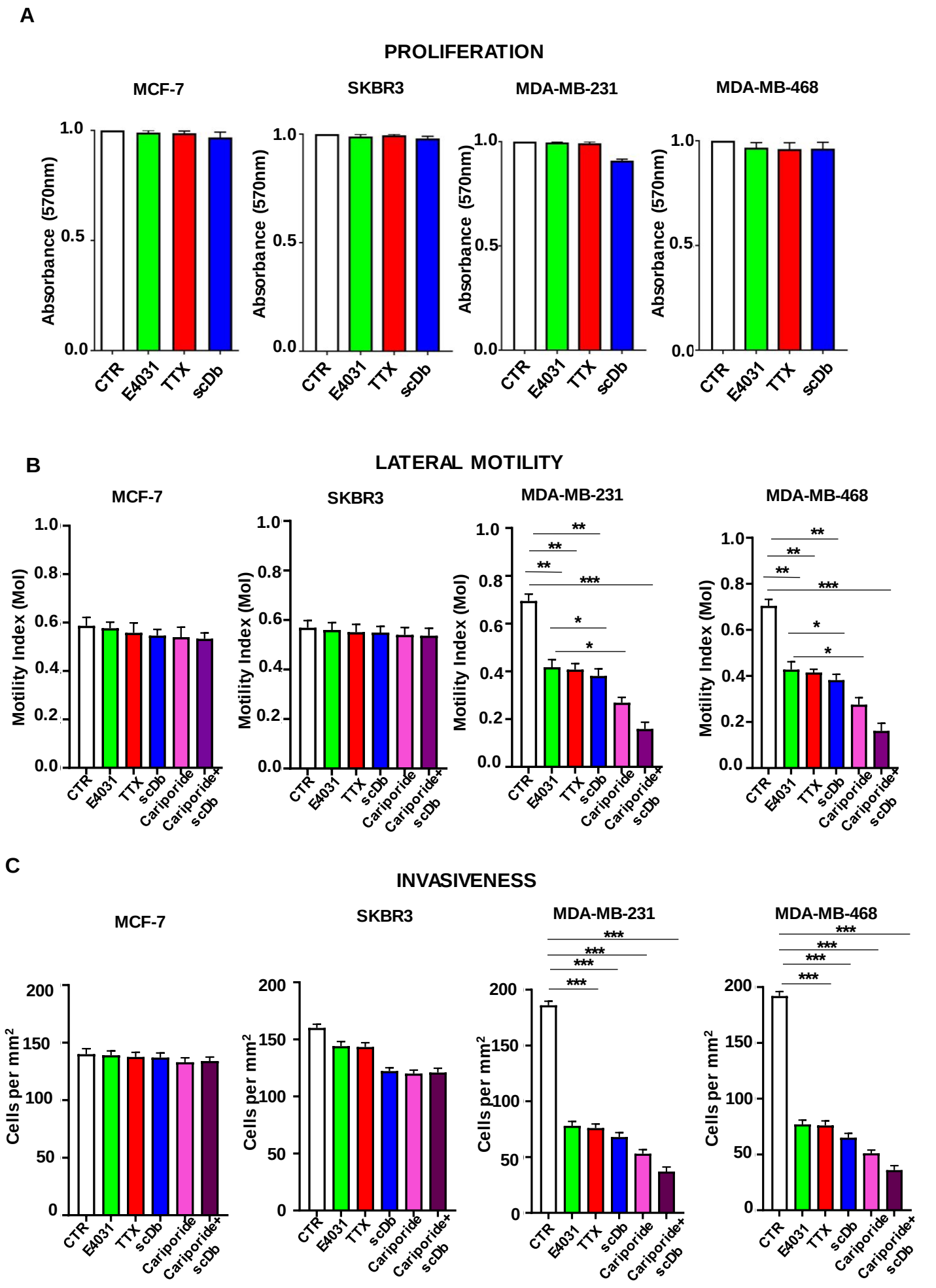
A
PROLIFERATION
MCF-7
SKBR3
MDA-MB-231
MDA-MB-468
Absorbance (570nm)
1.0
0.5
0.0
CTR
E4031
TTX
scDb
B
LATERAL MOTILITY
Motility Index (MoI)
Cariporide
Cariporide+ scDb
C
INVASIVENESS
Cells per mm2
200
150
100
50
0

Figure 10

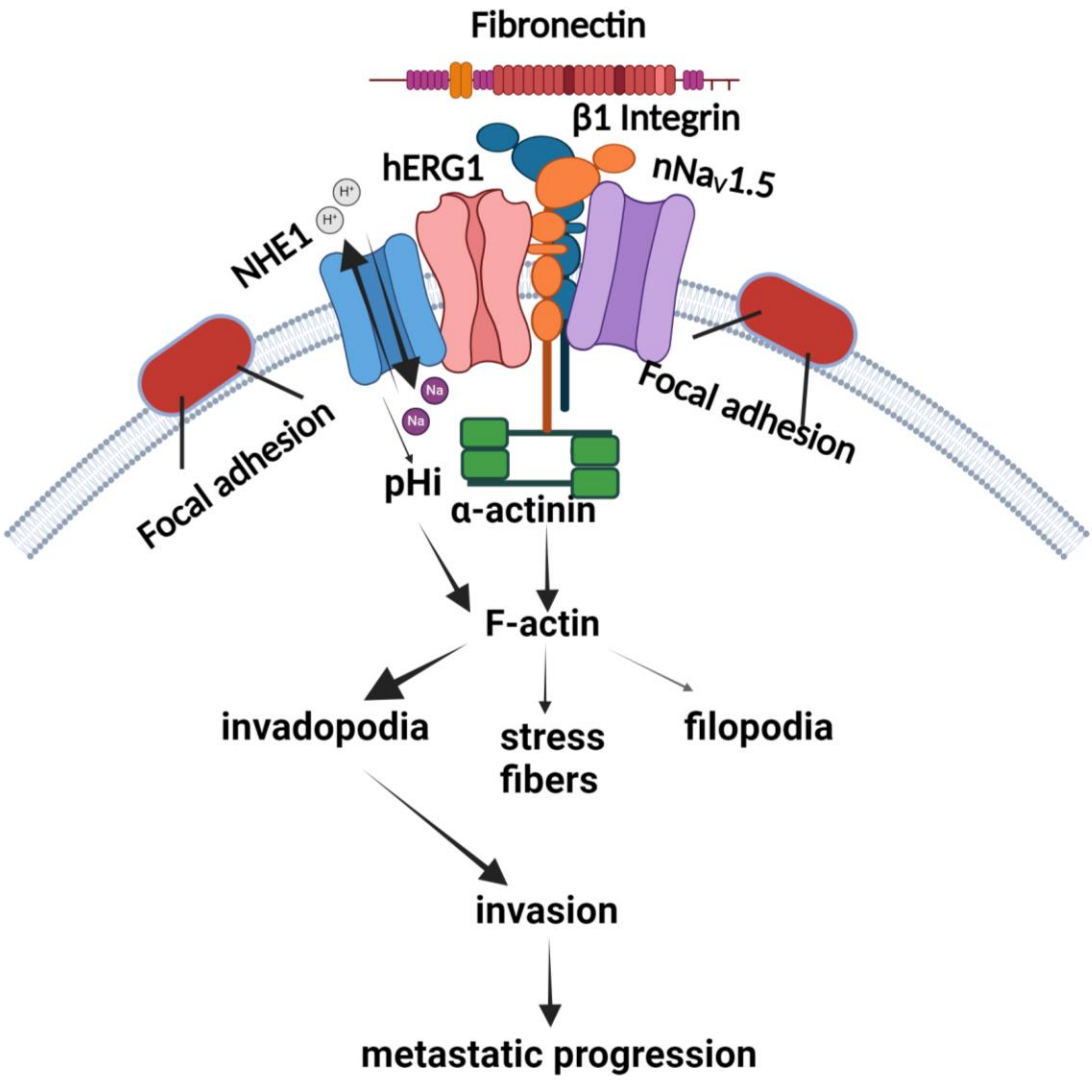
Fibronectin
β1 Integrin
hERG1
nNaV1.5
NHE1
H+
H+
Na
Na
Focal adhesion
Focal adhesion
pHi
α-actinin
F-actin
invadopodia
stress fibers
filopodia
invasion
metastatic progression

Figure 11